

# Urban impacts on deep convection development in the Seoul metropolitan area: A case modeling study of a scattered convective precipitation event

Seong-Ho Hong | Jong-Jin Baik<sup>ID</sup>

School of Earth and Environmental Sciences, Seoul National University, Seoul, South Korea

## Correspondence

Jong-Jin Baik, School of Earth and Environmental Sciences, Seoul National University, Seoul 08826, South Korea.  
 Email: [jbaik@snu.ac.kr](mailto:jbaik@snu.ac.kr)

## Funding information

National Research Foundation of Korea, Grant/Award Numbers:  
 2021R1A2C1007044, RS-2025-00562044

## Abstract

Storms causing urban precipitation can develop from interactions between various local forcings in and around cities. This study investigates urban impacts on storm development and precipitation and their interactions with topographic impacts for a scattered convective shower event in the Seoul metropolitan area (SMA), South Korea. For this, ensemble simulations with land use map and topography of the SMA and additional sets of ensemble simulations in which the urban area, urban heating, urban drag, or topography in the SMA is removed are conducted using the Weather Research and Forecasting model. The precipitation amount in Seoul for this event substantially increases by urban impacts. This precipitation increase is mainly attributed to the urban heat island (UHI) which helps convective cells develop into strong storms by increasing the temperature gradient at the front of cold outflows and enhancing updrafts there. Although weak urban breeze is induced by the UHI, it does not play crucial roles in precipitation for this event. Meanwhile, the urban drag causes marginal changes in precipitation amount but delays precipitation evolution by about 1 hour. The interaction of topographic impacts with urban impacts also contributes to the development of strong storms in Seoul and increases precipitation in northeastern Seoul. This is attributed to the circulation induced by convection over the eastern mountains which suppresses precipitation development near the western coast by sea breeze in the morning and preserves the warm air. The preserved warm air later moves into Seoul along with the sea breeze and invigorates storm development in Seoul in the late afternoon.

## KEY WORDS

cold outflow, urban drag, urban heat island, urban precipitation, urban-topographic interaction

## 1 | INTRODUCTION

Precipitation is one of the weather phenomena that are associated with the largest economic damage and/or highest casualty count (MOIS, 2024; NCEI, 2024; WMO, 2021).

Heavy precipitation poses great risks especially to cities, as urban surfaces paved with impervious materials likely enhance surface runoff and increase flood risks (Chen et al., 2017; Oke et al., 2017). With the proportion of urban population being projected to increase in future

(UN, 2019), the importance of accurate predictions of precipitation in cities keeps increasing. This necessitates better understanding of factors influencing urban precipitation. It has been shown for many cities that precipitation amounts in and/or downwind of cities tend to be larger than those in other surrounding areas (Changnon et al., 1977; IPCC, 2023; Liu & Niyogi, 2019). This suggests that urban areas themselves do affect precipitation and their impacts can be an important factor in precipitation in cities, in addition to other well-known influential factors such as synoptic forcings, environmental conditions, and geographical elements.

Three factors were suggested to be mainly responsible for urban impacts on precipitation (Han et al., 2014): the urban heat island (UHI) (e.g., Wu et al., 2019; Yang et al., 2017) which enhances low-level instability and convection, the large urban surface roughness and resultant urban drag (e.g., Bornstein & LeRoy, 1990; Dou et al., 2015) which decelerate and/or perturb winds, and the abundant anthropogenic aerosols (e.g., Fan et al., 2018; Rosenfeld, 2000) which change in-cloud microphysical processes. How urban impacts affect precipitation has been revealed through numerical simulations considering an inland city on plains where urban impacts are less disrupted by other local forcings. Precipitation can be induced by the UHI-induced circulation/flow (Baik et al., 2001, 2007; Han & Baik, 2008; Rozoff et al., 2003). While the induced precipitation system is likely to concentrate precipitation within urban areas under calm conditions (e.g., Zhang et al., 2022), it was also reported that the precipitation system can develop into an organized system and produce significant precipitation tens of kilometers downwind of city under moderate background winds (Hong et al., 2024). In addition, precipitation systems can be modified as they pass through a city or its surrounding areas. They can be invigorated by the influence of the UHI (Naylor, 2020; Naylor & Mulholland, 2023) or urban aerosols (Han et al., 2012; Schmid & Niyogi, 2017). Also, the movements of precipitation systems can be diverted by the UHI-induced convergent flows and urban-induced changes in cold outflows (Lin et al., 2021). For a supercell storm, it was reported that the strength and track of mesocyclone may be changed by urban impacts (Reames & Stensrud, 2018).

Many metropolitan cities are situated in complex geographical conditions where the roles of urban impacts can be changed by interacting with the impacts of geographical elements. Studies on coastal cities showed that the UHI impacts enhance sea breeze and associated moisture transport toward urban areas, increasing precipitation in urban areas (e.g., Argüeso et al., 2016; Doan et al., 2023; Kusaka et al., 2014; Sun et al., 2021). The UHI impacts

hamper farther inland penetration of sea breeze and associated moisture transport beyond urban areas, which reduces or weakens precipitation in inland areas (e.g., Hu et al., 2021; Kusaka et al., 2014, 2019; Lin et al., 2011). Meanwhile, studies on cities located near mountains showed various ways of interactions between urban and topographic impacts. Urban dry island impacts can delay convection initiation over mountain slopes downwind of cities by reducing moisture transport toward the mountains (Freitag et al., 2018; Lin et al., 2011). If precipitation is triggered over mountain slopes, urban drag impacts decelerate downslope cold outflows from the precipitation system, which can increase moisture convergence and enhance precipitation (He et al., 2023; Yang et al., 2019). In addition, mountain–plain circulations may increase near-surface wind speed and sensible heat flux in urban areas, further enhancing the UHI-induced precipitation increases (Sun et al., 2021). The mountains downwind of a city may also help urban-initiated storm strongly develop through the back-building process by blocking the storm's outflows (Yin et al., 2020). While there is a general consensus about the processes associated with urban–sea interaction impacts, those associated with urban–topographic interaction impacts are reported to be diverse, implying the necessity for further investigation.

The Seoul metropolitan area (SMA), South Korea (Figure 1a–c), is one of the largest metropolitan areas in East Asia, being comprised of the capital Seoul and nearby suburban and rural areas. The SMA has a total population of ~26 million and a population density of ~2300 km<sup>-2</sup> (KOSIS, 2024) and is characterized by complex geographical conditions. The Yellow Sea is located west of the SMA, and high mountains with peak heights higher than 1000 m are located in the eastern SMA and east of the SMA. In the SMA, the Han River with a width of ~1 km traverses Seoul and some modest mountains are present. In these regards, the SMA can be a good place to investigate complex interactions between urban impacts and the impacts of geographical elements.

The urban impacts on precipitation in the SMA were examined by a few numerical modeling studies. Kim et al. (2021) performed regional climate simulations, changing the anthropogenic heat intensity and building height. They revealed that in the SMA, the enhanced anthropogenic heat can increase precipitation throughout the day due to the UHI impacts while the increased building height can have contrasting effects in the daytime and nighttime due to the impacts of urban cool island and urban drag. Choi and Lee (2021) conducted real-case simulations of a sea breeze-initiated precipitation event, with different anthropogenic heat intensities and building heights and with the presence/absence of

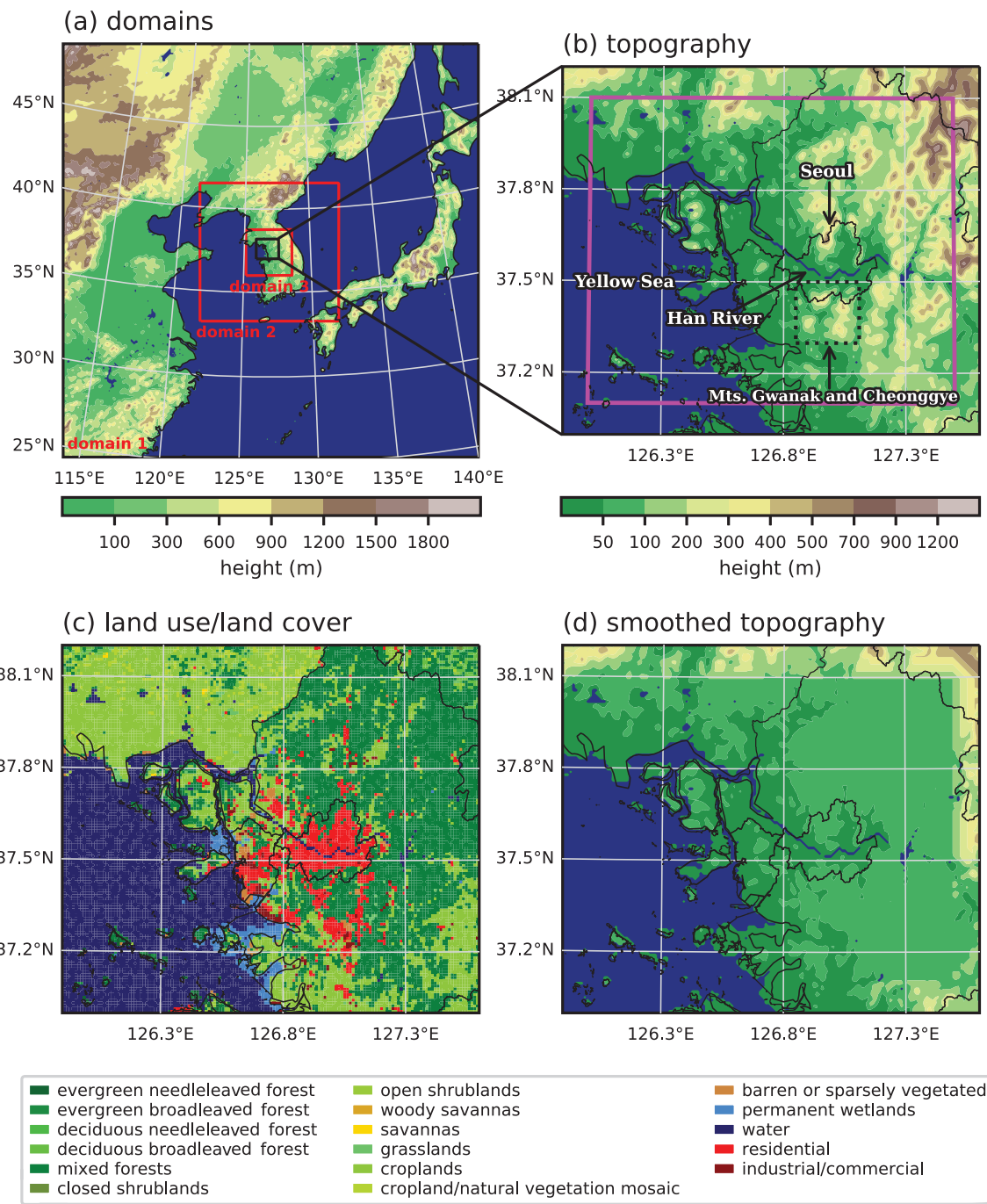


**FIGURE 1** (a) Model domain configuration. (b) Topographic map and (c) LULC map of the SMA for the URBAN control simulation. The pink box in (b) represents the main analysis region. (d) Topographic map of the SMA for the NO-TOPO control simulation. [Colour figure can be viewed at [wileyonlinelibrary.com](http://wileyonlinelibrary.com)]

the Yellow Sea. They showed that the urban characteristics and the sea breeze from the Yellow Sea affect the amount and location of precipitation in the SMA. Despite the contributions of previous studies, several questions about urban impacts on precipitation in the SMA remain to be answered. For example, how the respective UHI impacts and urban drag impacts quantitatively contribute to storm development and precipitation in the SMA

remains unclear. While examinations with different urban parameter values show urban impacts with different UHI and urban drag intensities, it is difficult to isolate each of the UHI and urban drag impacts since urban parameters collectively contribute to both the impacts. In addition, how urban-topographic interaction changes storm development and precipitation has not been investigated yet in the SMA. An investigation of this interaction in

the SMA may give some additional insights into storm development in other large cities under complex geographical conditions.

In this study, we look into urban impacts on storm development and precipitation during a convective shower event in the SMA using ensemble simulations. The UHI impacts and urban drag impacts on storm development and precipitation are separately analyzed and compared with each other, and the interaction of urban impacts with topographic impacts is also analyzed. In Section 2, the datasets used in this study are introduced and precipitation case and experimental setup are described. In Section 3, the results and discussion are provided. In Section 4, a summary and conclusions are given.

## 2 | METHOD

### 2.1 | Datasets

Reanalysis and observational datasets used for analysis are described here. The European Centre for Medium-Range Weather Forecasts Reanalysis version 5 (ERA5) data (Hersbach et al., 2020) with a temporal resolution of 1 hour and a horizontal resolution of  $0.25^\circ$  are used to present synoptic conditions for the precipitation event of interest. The constant altitude plan position indicator (CAPPI) data at  $z = 1.5$  km from the multi-radar composites are used to show the evolution of convective cells in this event. The temporal and horizontal resolutions of the CAPPI data are 10 minutes and 1 km, respectively. The 1-min precipitation and temperature data from surface observation stations in the SMA are used to examine spatial distributions of accumulated precipitation amount and near-surface temperature before precipitation.

### 2.2 | Case description

On 4 August 2019, scattered convective showers occurred in and around Seoul in the late afternoon and early evening. Figure 2a shows the spatial distribution of accumulated precipitation amount observed by the rain gauges in the SMA on this day. Precipitation occurred mainly in northeastern Seoul, in southwestern Seoul, and south of Seoul. This precipitation is accumulated largely within  $\sim 2$  hours, recording a 2-hour accumulated precipitation amount of 48.5 mm at a station in northeastern Seoul. The associated synoptic conditions are presented in Figure 3. On this day, the well-developed North Pacific high is expanded to the Korean Peninsula from the east (Figure 3a,b). Due to the influence of this North Pacific high, heat waves persisted for 5 days (from 2 to 6 August

2019) and the daily maximum 2-m temperature on the day of interest was  $34.4^\circ\text{C}$  in Seoul. In the lower troposphere (Figure 3a), warm and moist air is transported to the Korean Peninsula from the southeast along the edge of the North Pacific high and winds are very weak ( $< 2 \text{ m}\cdot\text{s}^{-1}$ ) in the SMA. In the middle troposphere (Figure 3b), warm and moist air is transported toward the Korean Peninsula by southerlies of  $\sim 8 \text{ m}\cdot\text{s}^{-1}$ . Under these conditions, the Korea Meteorological Administration forecasted showers over the inland regions of South Korea.

The evolution of convective storms in the SMA is shown in Figure 4a-d which presents the fields of observed radar reflectivity at different times. At 1540 LST (UTC + 9 hours) (Figure 4a), weak convective cells appear south of Seoul (green arrow). These cells develop, and around them, new cells appear in southwestern Seoul (blue arrow) and in northeastern Seoul (red arrow) (Figure 4b). At 1640 LST (Figure 4c), these new convective cells in southwestern Seoul and in northeastern Seoul develop into strong convective storms. These storms merge with each other and produce heavy precipitation during  $\sim 2$  hours (not shown), resulting in the precipitation accumulation in northeastern Seoul (Figure 2a). These storms weaken and almost dissipate at around 1840 LST (Figure 4d).

### 2.3 | Model description and experimental design

The precipitation event in the SMA is simulated using the Weather Research and Forecasting (WRF) model version 4.1.3 (Skamarock et al., 2019). Three one-way nested domains centered on the SMA are used (Figure 1a). The horizontal grid spacings of these domains are 9, 3, and 1 km. The height of the domain top is  $\sim 21$  km ( $\sim 50$  hPa). Total 50 vertical layers are used, and 10 of them are below  $z = 2$  km. The vertical grid spacing is stretched from 53 to 444 m with increasing height. For lateral boundary conditions of the outermost domain and initial conditions of all domains, the hourly ERA5 data are used. The model is integrated for 24 hours from 0000 LST 4 August 2019. The 10-min output data of simulations are used for analysis. The physics parameterization options used in this study are as follows: the WRF double-moment 6-class (WDM6) microphysics scheme (Lim & Hong, 2010), the University of Washington planetary boundary layer scheme (Bretherton & Park, 2009), the revised MM5 surface layer scheme (Jiménez et al., 2012), the unified Noah land surface model (Tewari et al., 2004), the Dudhia shortwave radiation scheme (Dudhia, 1989), and the Rapid Radiative Transfer Model (RRTM) longwave radiation scheme (Mlawer et al., 1997).

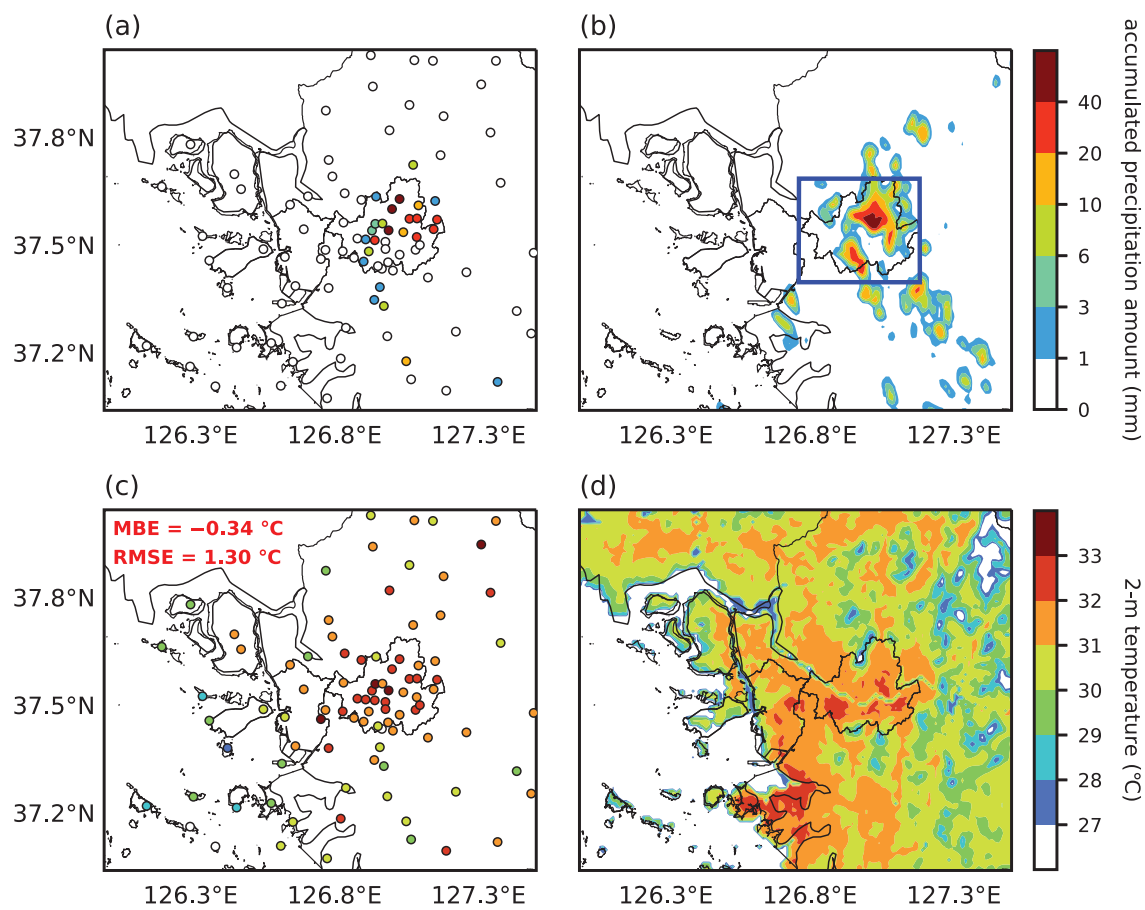


**FIGURE 2** Spatial distributions of (a,b) accumulated precipitation amount on 4 August 2019 and (c,d) 2-m temperature at 1100 LST on this day (a,c) for the observation and (b,d) for the URBAN control simulation. The blue box in (b) represents the Seoul region which is used for the analysis in Figures 10–12. The mean bias error (MBE) and root-mean-squared error (RMSE) of 2-m temperature in the SMA at the time are given in (c). The simulated temperature is bilinearly interpolated when quantitatively compared with the observed temperature. [Colour figure can be viewed at [wileyonlinelibrary.com](https://wileyonlinelibrary.com)]

The Seoul National University Urban Canopy Model (SNUUCM; Ryu et al., 2011) is employed to represent interactions between urban areas and the overlying atmosphere. The SNUUCM is a single-layer urban canopy model that calculates various physical processes in a street canyon such as the reflection of shortwave and longwave radiation within the canyon, a shadow cast by a building, turbulent exchanges between built-up surfaces (i.e., roof, two walls, and road) and the adjacent air, and heat conduction through subsurface layers. The surface fluxes from the built-up portion of urban areas are calculated by the SNUUCM and those from the natural portion of urban areas are calculated by the Noah land surface model. The total surface fluxes from urban areas are calculated as the area-weighted average of the fluxes from the built-up and natural portions. The SNUUCM was evaluated through several studies (Grimmond et al., 2010, 2011; Jongen et al., 2024; Lipson et al., 2024; Ryu et al., 2011, 2012). The land use/land cover (LULC) map used in this study

is presented in Figure 1c. In the SMA, the LULC map constructed by Ryu and Baik (2013) based on geographic information system data from the Korea Ministry of Environment is used. Outside of the SMA, the Moderate Resolution Imaging Spectroradiometer (MODIS) LULC map is used. The urban parameters for two urban categories, which are “residential” and “industrial/commercial”, are determined following those of Ryu and Baik (2013), and are listed in Table 1.

The simulations conducted using the LULC map in Figure 1c are named URBAN. To investigate urban impacts on the precipitation event, simulations with urban areas being replaced with croplands in the main analysis region (pink box in Figure 1b) in domain 3 are conducted and named NO-URBAN. Location and/or timing of individual simulated convective storms can sensitively change with simulation setting (e.g., Forster et al., 2024; Kusaka et al., 2009), which can hinder robust examinations of urban impacts in convective precipitation events by a

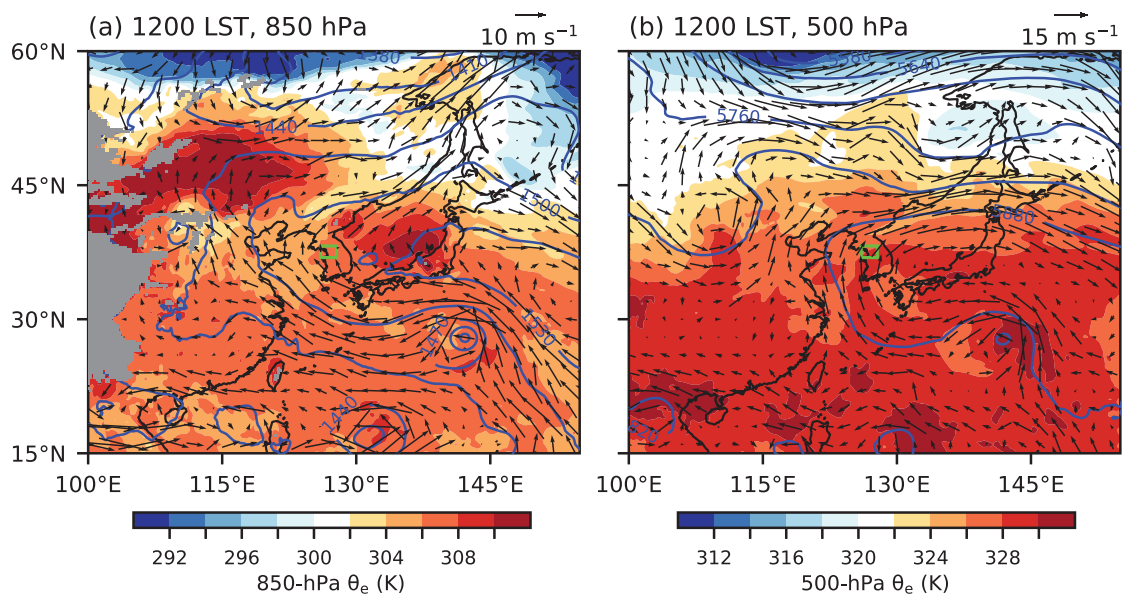


**FIGURE 3** Fields of geopotential height (blue contours), equivalent potential temperature (shades), and wind vector (arrows) at (a) 850-hPa and (b) 500-hPa levels at 1200 LST 4 August 2019. The gray-shaded area in (a) indicates the area where surface pressure is lower than 850 hPa. The green squares indicate the location of the SMA. [Colour figure can be viewed at [wileyonlinelibrary.com](http://wileyonlinelibrary.com)]

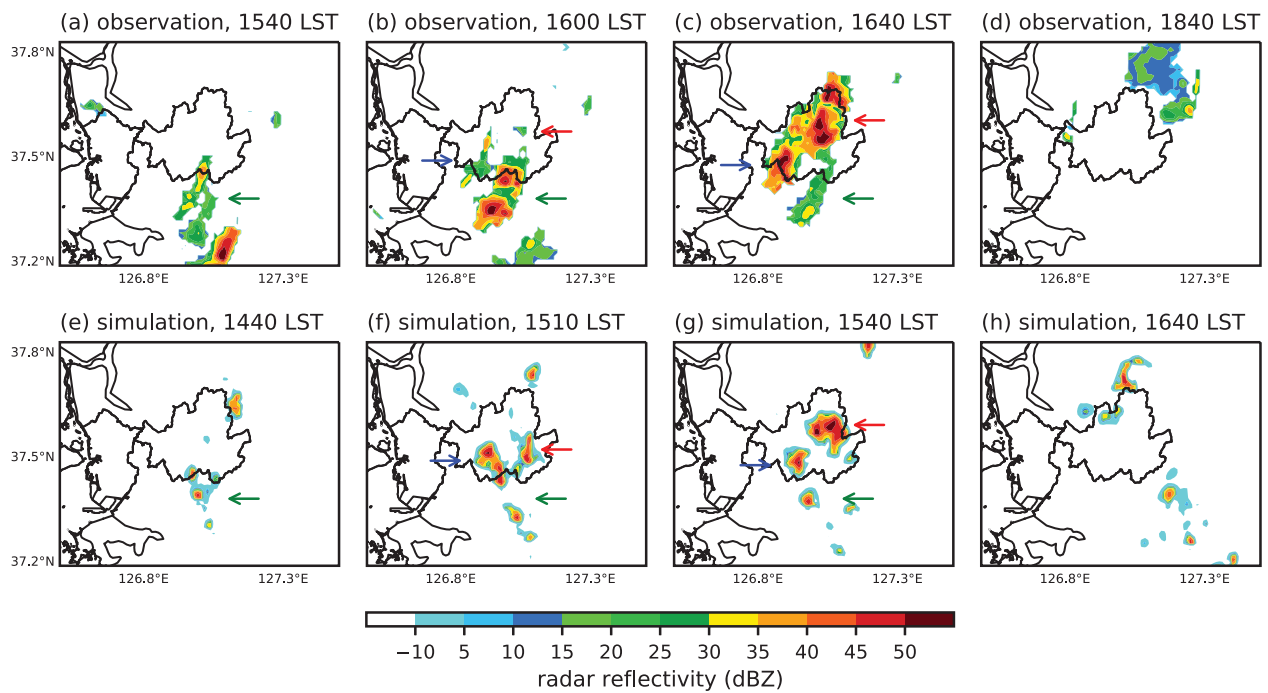


**FIGURE 4** Fields of radar reflectivity (the CAPPI at  $z=1.5$  km) at different times (a-d) for the observation and (e-h) for the URBAN control simulation. The green, blue, and red arrows indicate the convective cells south of Seoul, in southwestern Seoul, and in northeastern Seoul, respectively. [Colour figure can be viewed at [wileyonlinelibrary.com](http://wileyonlinelibrary.com)]

comparison in a single pair of urban and nonurban simulations. For a more reliable examination of urban impacts on precipitation, additional simulations using four different double-moment microphysics schemes are conducted

for each of the URBAN and NO-URBAN simulations. These microphysics schemes are the Thompson scheme (Thompson et al., 2008), the Morrison double-moment scheme (Morrison et al., 2009), the predicted particle

**TABLE 1** Settings of urban parameters and anthropogenic heat for the two urban categories.

Parameter	Residential	Industrial/ commercial
Built-up area fraction	0.815	0.9
Natural area fraction	0.185	0.1
Mean building height	10 m	15 m
Canyon aspect ratio	0.5	1
Roof fraction	0.6	0.6
Mean anthropogenic heat flux	$21 \text{ W m}^{-2}$	$33 \text{ W m}^{-2}$

properties (P3) scheme (Morrison & Milbrandt, 2015) that prognoses the cloud droplet number concentration, and the ice-spheroids habit model with aspect-ratio evolution (ISHMAEL) scheme (Jensen et al., 2017). The setting of the control simulation and the way of constructing ensemble simulations were determined after a large number of tests for different microphysics parameterizations, boundary layer parameterizations, initial times of the simulations, and urban-related parameters. The microphysics scheme is chosen for the construction of ensemble simulations based on the test results, in order to retain less ensemble spreads in location and/or timing of simulated convective cells. Detailed investigation of model uncertainty arising from the choice of physics parameterization schemes (e.g., Jin & Baik, 2025) for scattered convective shower cases would be greatly beneficial to proper selection of physics schemes.

### 3 | RESULTS AND DISCUSSION

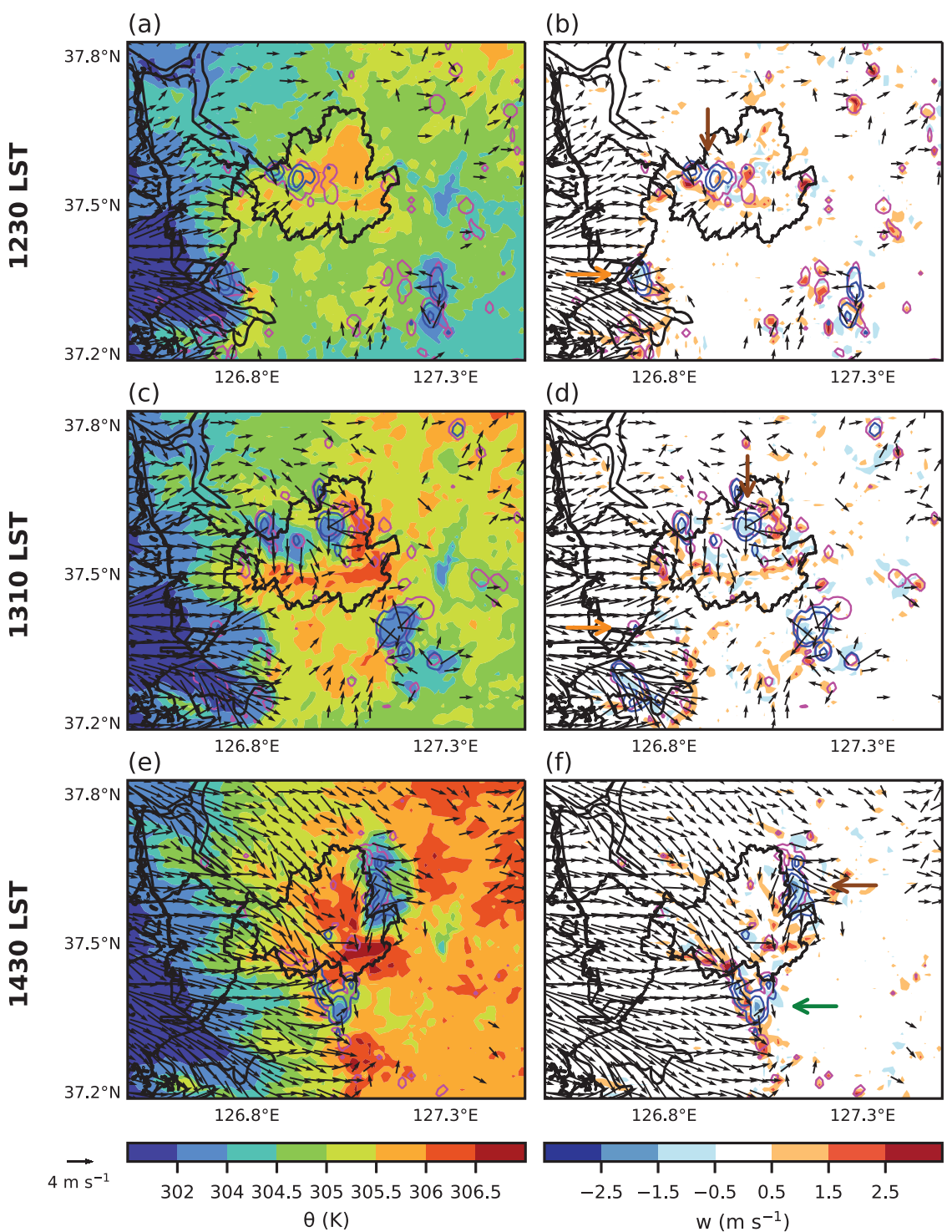
#### 3.1 | Convective storm evolution

Figure 2b shows the spatial distribution of accumulated precipitation amount on 4 August 2019 for the URBAN control simulation. The simulated precipitation is mainly accumulated in northeastern Seoul, in southwestern Seoul, and south of Seoul (Figure 2b), overall agreeing with the observed precipitation (Figure 2a). The simulated evolution of convective storms is shown in Figure 4e–h. At 1440 LST (Figure 4e), convective cells develop south of Seoul (green arrow). The strong storm in southwestern Seoul appears (blue arrow) and a new convective cell is initiated in southeastern Seoul (red arrow) at around 1500 LST (Figure 4f). The new convective cell develops into a strong storm (main storm) in northeastern Seoul at 1540 LST with the presence of the strong storm in southwestern Seoul (Figure 4g), which is similar to the observed evolution of storms at around 1640 LST (Figure 4c). The simulated storms produce heavy precipitation during  $\sim 1$

hour, which is  $\sim 1$  hour shorter than the duration of the observed storms ( $\sim 2$  hours), and then dissipate at around 1640 LST (Figure 4h). Despite the earlier ( $\sim 1$  hour) advent and shorter ( $\sim 1$  hour) duration of the strong convective storms in the simulation, the overall evolution and location of the observed storms in and around Seoul are well reproduced in the simulation.

Figure 2c,d shows the spatial distributions of observed and simulated 2-m temperatures at 1100 LST before appreciable precipitation begins in the SMA. The observed temperature near the western coast ( $\sim 27\text{--}31^\circ\text{C}$ ) tends to be relatively low compared with that in other land regions ( $\sim 29\text{--}33^\circ\text{C}$ ), being influenced by the Yellow Sea (Figure 2c). The observed temperature in Seoul ( $\sim 31\text{--}34^\circ\text{C}$ ) is further higher than that in other land regions, exhibiting the UHI. When the observation stations in the SMA are classified into urban and rural stations based on the LULC map (Figure 1c), the mean urban–rural contrast in observed 2-m temperature at this time is  $1.30^\circ\text{C}$ . The spatial pattern of simulated temperature also features relatively lower temperature near the coast and relatively high temperature in Seoul, generally agreeing with the spatial pattern of observed temperature (Figure 2d). The mean bias error and root-mean-squared error are  $-0.34$  and  $1.30^\circ\text{C}$ , respectively, and the simulated urban–rural contrast in 2-m temperature is  $1.39^\circ\text{C}$  which is close to the observed contrast ( $1.30^\circ\text{C}$ ). This indicates that the URBAN control simulation reliably reproduces the near-surface temperature distribution before precipitation. The overall agreements in the temperature and precipitation (Figures 2 and 4) encourage us to examine possible urban impacts on the storm development and precipitation for this precipitation event.

The early-afternoon evolution of local winds and convective cells in the SMA before the advent of the strong convective storms is examined. Figure 5 presents the fields of total water (liquid and ice) path, precipitation rate, potential temperature and wind vector at the lowest model level, and vertical velocity at  $z=1 \text{ km}$  at different times in the early afternoon in the URBAN control simulation. The wind vectors are plotted only for the winds stronger than  $2 \text{ m s}^{-1}$ . At 1230 LST, sea breeze blows from the western coast and urban breeze weakly develops near the northwestern and southwestern border of Seoul (Figure 5a). Updrafts are generated along the front of sea breeze southwest of Seoul, and convective cells develop there (orange arrow) (Figure 5b). Meanwhile, another convective cells develop in western Seoul (brown arrow, Figure 5b) due to the updrafts associated with river breeze from the Han River (not shown). As the convective cells near the western coast (orange arrow) produce precipitation, the sea breeze southwest of Seoul is enhanced by the precipitation-produced cold outflow (Figure 5c). This is



**FIGURE 5** Fields of (a,c,e) potential temperature at the lowest model level (shades) and (b,d,f) vertical velocity at  $z=1$  km (shades) at (a,b) 1230, (c,d) 1310, and (e,f) 1430 LST for the URBAN control simulation. Fields of total water path (pink contours, at  $0.3\ kg\cdot m^{-2}$ ), precipitation rate (blue contours, at 1 and  $5\ mm\cdot hr^{-1}$ ), and wind vector at the lowest model level (black arrows,  $> 2\ m\cdot s^{-1}$ ) are also presented. The orange, brown, and green arrows in (b,d,f) indicate the different convective cells explained in the text. [Colour figure can be viewed at [wileyonlinelibrary.com](http://wileyonlinelibrary.com)]

similar to the enhancement of thermally induced breeze by the breeze-triggered precipitation, which is reported by Rieck et al. (2015). A part of the convective cells in western

Seoul moves and develops eastward (brown arrow), as their cold outflow lifts the warm urban air located east (Figure 5c) and generates updrafts (Figure 5d). At 1430

LST (Figure 5e), the sea breeze penetrates into Seoul and reaches Mts. Gwanak and Cheonggye (see Figure 1b). The prominently warm urban air is found in Seoul, with its potential temperature reaching 306 K. Along the sea breeze front south of Seoul, linearly organized updrafts are generated, and above the front near Mts. Gwanak and Cheonggye, strong convective cells develop (green arrow) (Figure 5f). The convective cells originating from western Seoul (brown arrow) are located near the northeastern border of Seoul at 1430 LST, producing precipitation and accompanying cold pool (Figure 5e).

The convective cells near Mts. Gwanak and Cheonggye lead to the strong storm in southwestern Seoul, and this storm and the prominently warm urban air play important roles in the development of the strong storm in northeastern Seoul. Figure 6 is the same as Figure 5 but at different times in the late afternoon when the strong convective storms develop in Seoul. The convective cells originally located near Mts. Gwanak and Cheonggye develop into the strong storm in southwestern Seoul (blue arrow) (Figure 6a). As the cold outflow from the storm in southwestern Seoul, the sea breeze penetrating into Seoul, and the cold outflow from the convective cells near the northeastern border of Seoul (brown arrow) converge with each other in southeastern Seoul, a new convective cell is initiated there (red arrow) (Figure 6b). This new convective cell rapidly develops into the strong storm in northeastern Seoul (Figure 6c) as its cold outflow lifts the warm urban air and generates strong updrafts (Figure 6d). The strong updrafts due to the convergence of cold outflows from the southwestern storm and the new convective cell also contribute to the development of the new convective cell into strong storm. This northeastern storm (red arrow) further develops (Figure 6e) as its cold outflow keeps lifting the warm urban air in northern Seoul (Figure 6f). These two storms, one in southwestern Seoul and the other in northeastern Seoul, are mainly responsible for the large accumulated precipitation in the respective regions (Figure 2b).

The interplay between the warm urban air and the cold outflows from the two storms and its impacts on the strong development of the northeastern storm are well seen in Figure 7, which presents the vertical cross sections of potential temperature, vertical velocity, total and rain water mixing ratios, and wind vector along the line A-B and line C-D at 1530 LST. Along the line A-B (Figure 7a), strong cold pool and diverging outflows are found below each of the two storms in southwestern Seoul (blue arrow) and in northeastern Seoul (red arrow). The cold outflow from the southwestern storm generates strong updrafts at  $x \sim 10$  km, feeding the southwestern storm itself (Figure 7b). The cold outflows from the southwestern storm and the northeastern storm also

generate strong updrafts together at  $x \sim 23$  km, feeding the northeastern storm. Along the line C-D (Figure 7c,d), the cold outflow from the northeastern storm generates strong updrafts at  $x \sim 17$  km by lifting the warm urban air advected by the sea breeze in northeastern Seoul. These updrafts enable the northeastern storm to strongly develop and to produce significant precipitation in northeastern Seoul which is the main precipitation for this event. Similar to the above results, it was implied from previous studies that precipitation-produced cold outflows could be an important trigger for urban precipitation. Kusaka et al. (2019) reported that in their simulations, the cold outflow from mountain-induced precipitation advances toward an urban area and converges with the sea breeze, which leads to precipitation in the urban area. Li et al. (2017) showed that the downslope cold outflows from the mesoscale convective system over mountains play crucial roles in initiating deep convection at the border of central urban area of Beijing, China.

### 3.2 | Urban impacts on precipitation: UHI and urban drag impacts

Comparisons of the URBAN simulations with the NO-URBAN simulations reveal urban impacts on the storm development and precipitation in Seoul. Figure 8 shows the spatial distributions of accumulated precipitation amount for the NO-URBAN control simulation and urban-nonurban differences in accumulated precipitation amount for the control simulation and the ensemble simulations. Similar to the URBAN control simulation, in the NO-URBAN control simulation, considerable precipitation is accumulated in southwestern Seoul (Figure 8a) by a storm developing in southwestern Seoul near Mts. Gwanak and Cheonggye at around 1440 LST (not shown). This suggests that the storm in southwestern Seoul develops under the geographical influences (e.g., Mts. Gwanak and Cheonggye and sea breeze), even when urban impacts are absent. Meanwhile, in contrast with the URBAN control simulation, in the NO-URBAN control simulation, the large precipitation in northeastern Seoul is not produced (Figure 8a) since the northeastern storm does not develop. This indicates that urban impacts increase precipitation in northeastern Seoul in this precipitation event (Figure 8b), implying the importance of urban impacts on storm development there. This precipitation increase in northeastern Seoul occurs in the ensemble simulations as well as in the control simulation (Figure 8c), which corroborates the finding.

The UHI and urban drag are the well-known factors potentially causing urban impacts on precipitation. To examine the respective contributions of the UHI and

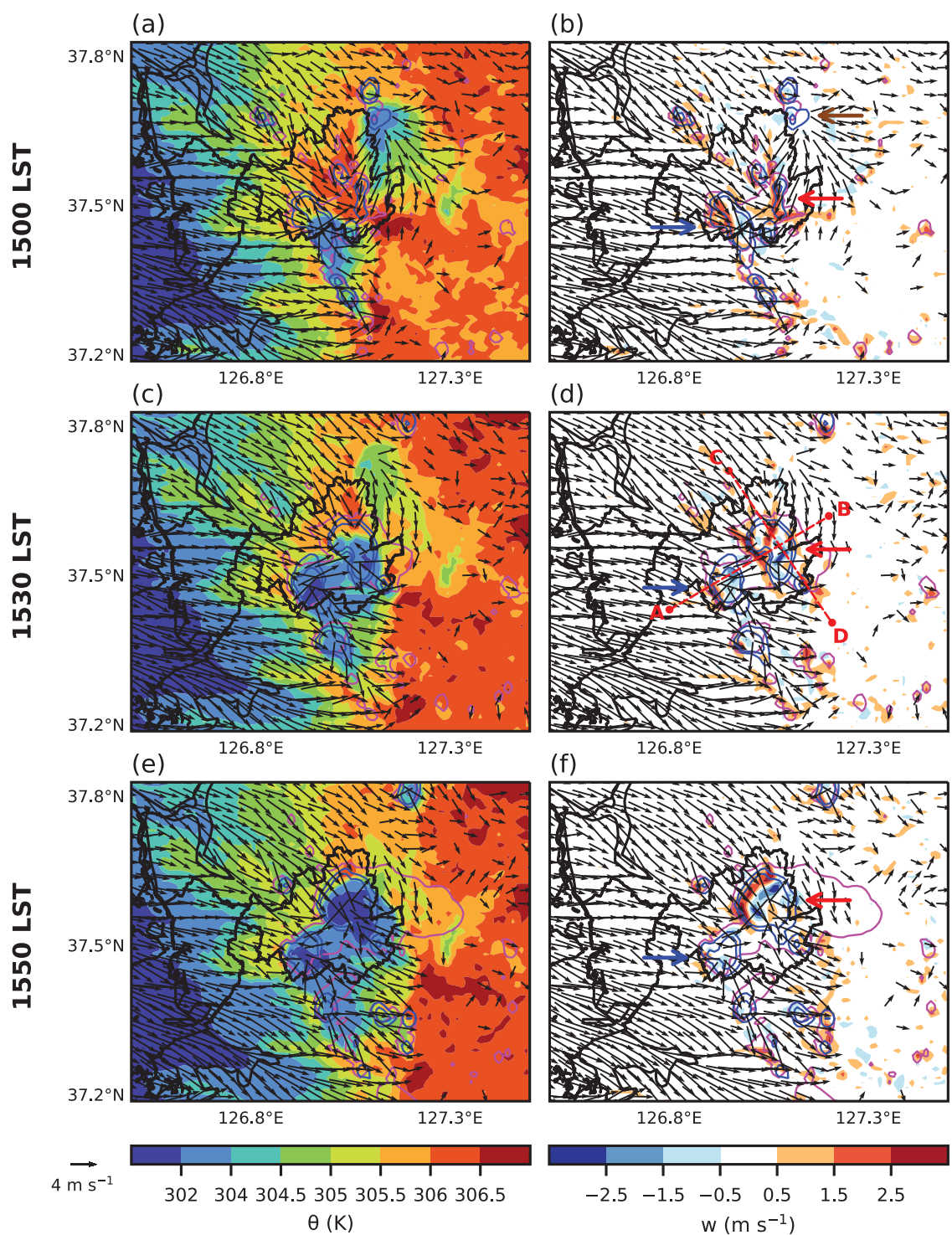


**FIGURE 6** As in Figure 5 but at (a,b) 1500, (c,d) 1530, and (e,f) 1550 LST. The brown, blue, and red arrows indicate the different convective cells or storms explained in the text. The lines A–B and C–D are the cross-section lines used for Figure 7. [Colour figure can be viewed at [wileyonlinelibrary.com](http://wileyonlinelibrary.com)]

urban drag impacts to the urban impacts on storm development and precipitation, two additional sets of ensemble simulations called the NO-UHI and NO-DRAG ensemble simulations are conducted. In the NO-UHI ensemble simulations, the sensible heat flux and surface temperature

of the natural (cropland) portion of urban areas are used as those of total urban areas. In the NO-DRAG ensemble simulations, the friction velocity of the natural portion of urban areas is used as that of total urban areas. Since urban enhancements in friction velocity in our simulations are

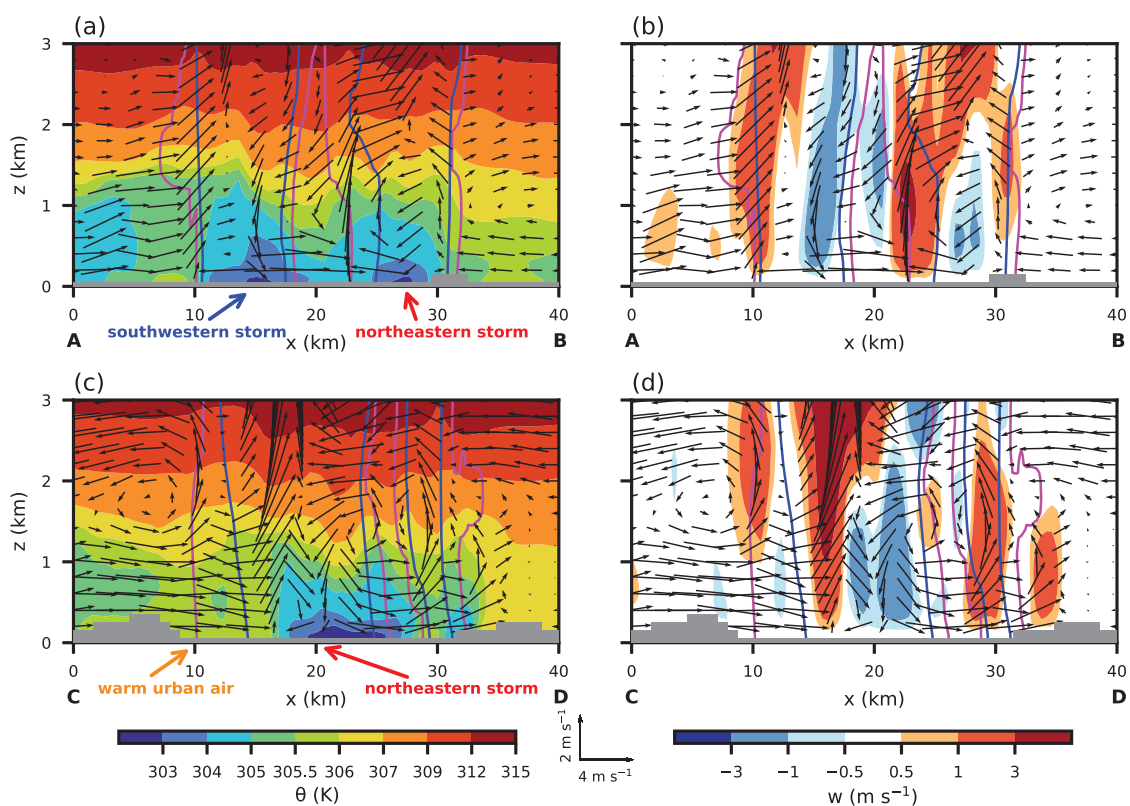


**FIGURE 7** Vertical cross sections of total water mixing ratio (pink contours, at  $0.01 \text{ g} \cdot \text{kg}^{-1}$ ), rain water mixing ratio (blue contours, at  $0.1 \text{ g} \cdot \text{kg}^{-1}$ ), wind vector (arrows), (a,c) potential temperature (shades), and (b,d) vertical velocity (shades) at 1530 LST along the (a,b) line A–B and (c,d) line C–D (see Figure 6d) for the URBAN control simulation. The gray-shaded areas represent the topography along the lines. [Colour figure can be viewed at [wileyonlinelibrary.com](http://wileyonlinelibrary.com)]

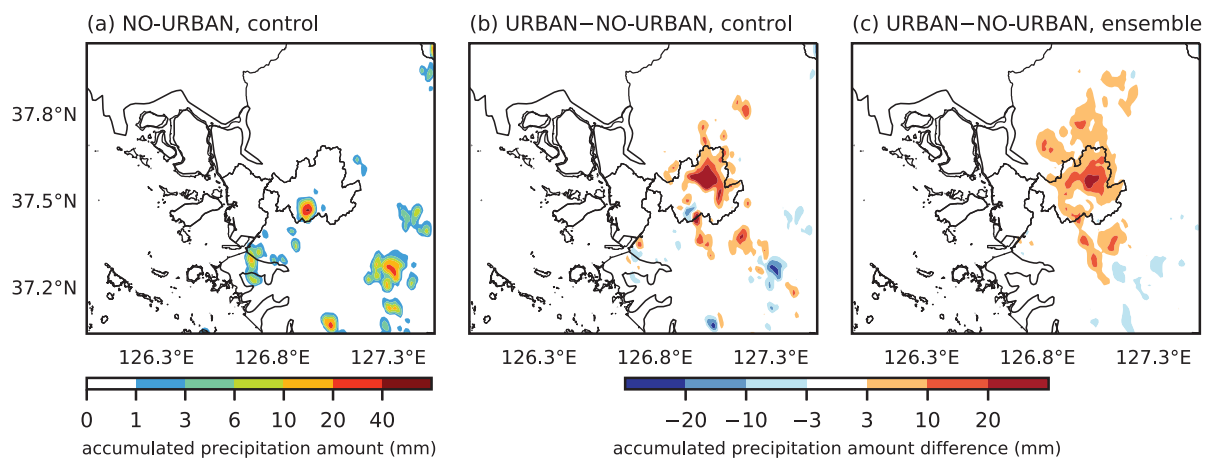


**FIGURE 8** Spatial distributions of (a) accumulated precipitation amount for the NO-URBAN control simulation and differences in accumulated precipitation amount (b) between the URBAN and NO-URBAN control simulations and (c) between the URBAN and NO-URBAN ensemble simulations. [Colour figure can be viewed at [wileyonlinelibrary.com](http://wileyonlinelibrary.com)]

contributed by urban thermal impacts as well as urban mechanical impacts, in the NO-DRAG ensemble simulations, the sensible heat flux and surface temperature of the natural portion are used when the friction velocity in

urban areas is calculated. All these modifications for the NO-UHI and NO-DRAG ensemble simulations are applied only to the urban grids within the main analysis region (Figure 1b) in the domain 3.

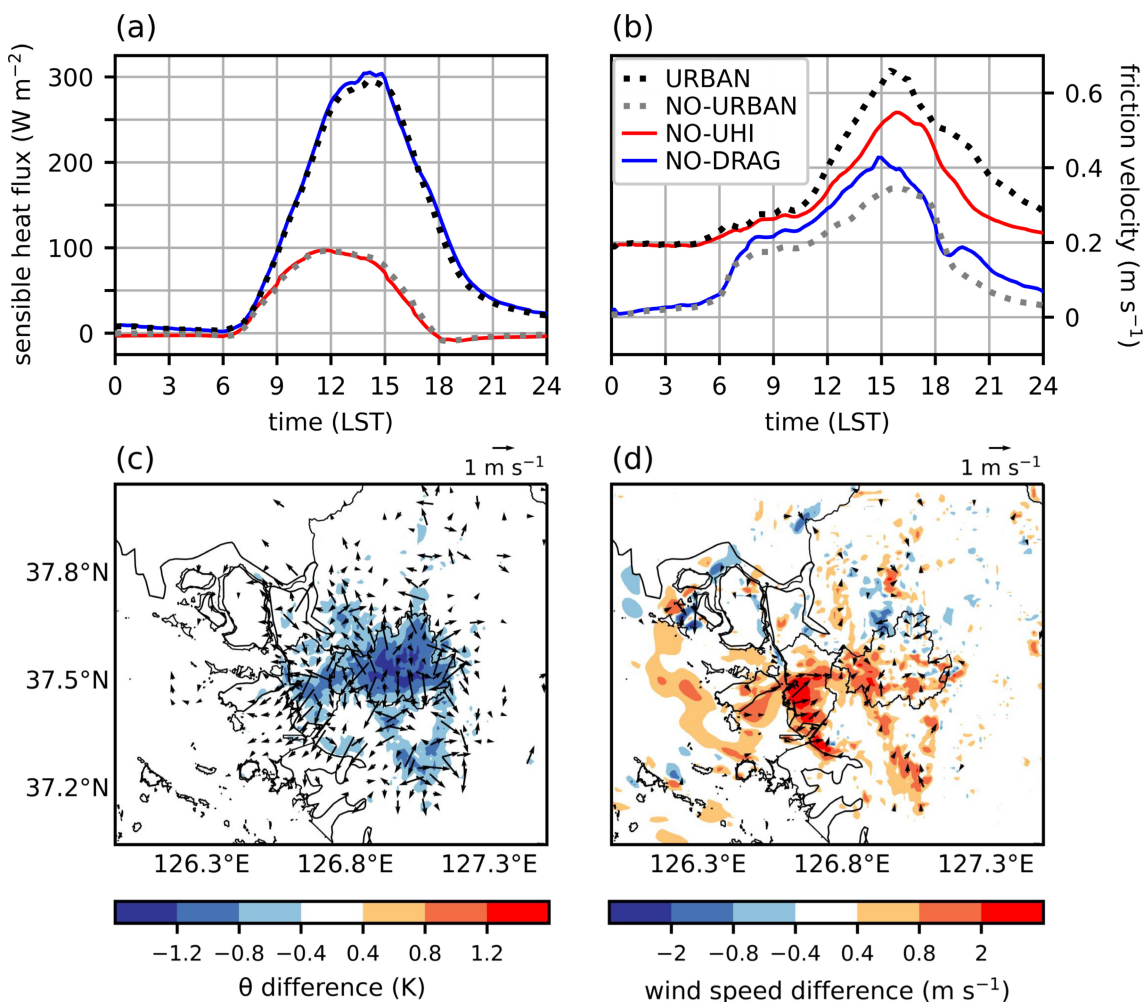


**FIGURE 9** Diurnal variations of (a) sensible heat flux and (b) friction velocity averaged over the urban grids in the main analysis region (pink box in Figure 1b) for the URBAN, NO-UHI, and NO-DRAG ensemble simulations and the corresponding cropland grids for the NO-URBAN ensemble simulations. Fields of (c) differences in potential temperature (shades) and wind vector (arrows,  $> 0.3 \text{ m s}^{-1}$ ) at the lowest model level averaged over 1100–1200 LST between the NO-UHI and URBAN ensemble simulations and (d) differences in wind speed (shades) and wind vector (arrows,  $> 0.3 \text{ m s}^{-1}$ ) at the lowest model level averaged over 1100–1200 LST between the NO-DRAG and URBAN ensemble simulations. [Colour figure can be viewed at [wileyonlinelibrary.com](http://wileyonlinelibrary.com)]

The sensible heat flux and friction velocity in the urban areas or corresponding areas in the SMA in the four sets of ensemble simulations are presented in Figure 9a,b. The sensible heat flux in the URBAN ensemble simulations is significantly larger than that in the NO-URBAN ensemble simulations (Figure 9a), resulting in the UHI in the SMA. The sensible heat flux in the NO-UHI ensemble simulations is very close to that in the NO-URBAN ensemble simulations while the sensible heat flux in the NO-DRAG ensemble simulations is very close to that in the URBAN ensemble simulations. The friction velocity in the URBAN ensemble simulations is higher than that in the NO-URBAN ensemble simulations (Figure 9b), resulting in the deceleration of winds above the urban areas in the SMA. The friction velocity in the NO-UHI ensemble simulations is close to that in the URBAN ensemble simulations

while the friction velocity in the NO-DRAG ensemble simulations is significantly reduced from that in the URBAN ensemble simulations. In contrast with the sensible heat flux, for the friction velocity, the differences between the URBAN (NO-URBAN) and NO-UHI (NO-DRAG) ensemble simulations are nonnegligible. These differences are mainly attributed to the presence/absence of urban-heated air at the lowest model level in the NO-DRAG/NO-UHI ensemble simulations (not shown), thereby being difficult to be prevented.

The UHI and its impacts are essentially removed in the NO-UHI ensemble simulations, and the urban drag impacts are significantly reduced in the NO-DRAG ensemble simulations. Figure 9c,d shows the fields of differences in potential temperature and wind vector between the NO-UHI and URBAN ensemble simulations and

differences in wind speed and wind vector between the NO-DRAG and URBAN ensemble simulations averaged over 1100–1200 LST before significant precipitation begins in the SMA. Compared with the URBAN ensemble simulations, the potential temperature in the urban areas is substantially decreased in the NO-UHI ensemble simulations, indicating that the UHI is effectively removed (Figure 9c). The wind differences directing outward from the urban areas indicate that the urban breeze induced by the UHI is also effectively removed. The magnitudes of wind differences are  $\sim 1 \text{ m}\cdot\text{s}^{-1}$  near the border of Seoul, showing that the urban breeze is weaker than the sea breeze ( $\sim 3 \text{ m}\cdot\text{s}^{-1}$ ) in the SMA. In the urban areas near the western coast of the SMA, the wind differences are directed from the land to the Yellow Sea. This indicates that the UHI impacts enhance the sea breeze. Compared with the URBAN ensemble simulations, the wind speed over the urban areas increases by  $\sim 1 \text{ m}\cdot\text{s}^{-1}$  in the NO-DRAG ensemble simulations, showing that the urban drag impacts are largely reduced (Figure 9d). The wind differences in the urban areas near the western coast are directed from the Yellow Sea to the land. This indicates that the urban drag impacts decelerate the sea breeze, counteracting the UHI impacts on the sea breeze.

Urban impacts on precipitation in Seoul and the respective contributions of the UHI and urban drag impacts to the urban impacts are examined. Figure 10a shows the accumulated precipitation amounts averaged over the Seoul region (blue box in Figure 2b) for the URBAN, NO-URBAN, NO-UHI, and NO-DRAG ensemble simulations. The precipitation amount in the NO-URBAN ensemble simulations is a fifth of that in the URBAN ensemble simulations, which suggests that the precipitation in Seoul is increased to  $\sim 5$  times by urban impacts for this convective shower event. The precipitation amount in the NO-UHI ensemble simulations is even smaller than that in the NO-URBAN ensemble simulations while the precipitation amount in the NO-DRAG ensemble simulations is very close to that in the URBAN ensemble simulations. This indicates that the UHI is the main factor causing the precipitation increase in Seoul for this convective shower event, rather than the urban drag. The relative importance of the UHI compared with the urban drag to urban impacts on precipitation was also reported by Rozoff et al. (2003) and Kusaka et al. (2019). The smaller precipitation in the NO-UHI ensemble simulations compared with the NO-URBAN ensemble simulations can be partly attributed to reduced moisture availability in Seoul due to urban dry island impacts.

The precipitation evolutions in Seoul for the four sets of ensemble simulations are compared in Figure 10b. The precipitation in the URBAN ensemble simulations begins at  $\sim 1200$  LST and is strongest at  $\sim 1600$  LST. In

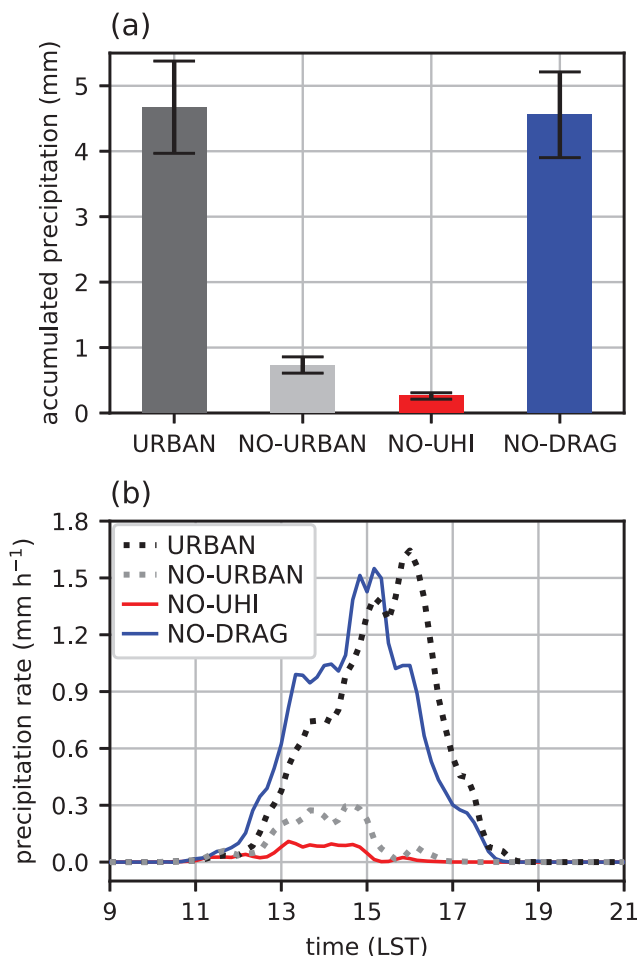


**FIGURE 10** (a) Accumulated precipitation amounts averaged over the Seoul region (blue box in Figure 2b) on 4 August 2019 and (b) time series of precipitation rate averaged over the Seoul region for the URBAN, NO-URBAN, NO-UHI, and NO-DRAG ensemble simulations. The whiskers in (a) indicate the  $\pm 1$  standard deviation ranges of the ensemble members. [Colour figure can be viewed at [wileyonlinelibrary.com](http://wileyonlinelibrary.com)]

the NO-URBAN ensemble simulations, the precipitation also begins at  $\sim 1200$  LST but ends early without being further intensified in the afternoon. This reflects that strong storms do not develop in Seoul in the afternoon in the NO-URBAN ensemble simulations. The precipitation in the NO-UHI ensemble simulations shows a temporal evolution similar to that of the precipitation in the NO-URBAN ensemble simulations, with weaker precipitation intensity. The precipitation in the NO-DRAG ensemble simulations evolves  $\sim 0.5\text{--}1$  hour earlier than that in the URBAN ensemble simulations. This 0.5–1 hour earlier evolution of precipitation is associated with an earlier inland penetration of sea breeze into the SMA where the deceleration by urban surfaces is reduced (not shown).

The differences in precipitation amount between the four sets of ensemble simulations are attributed to

the differences in storm development in Seoul in the afternoon. Figure 11 shows the contoured frequency by altitude diagrams of total water mixing ratio and vertical velocity in the Seoul region (blue box in Figure 2b) during 1300–1700 LST for the URBAN, NO-URBAN, NO-UHI, and NO-DRAG ensemble simulations. The contoured frequency is given in terms of the probability density function (PDF). In the URBAN ensemble simulations, a large amount of condensates ( $> 5 \text{ g kg}^{-1}$ ) and vigorous updrafts ( $> 10 \text{ m s}^{-1}$ ) are found above  $z=10 \text{ km}$  (Figure 11a,b), indicating the developments of deep and strong storms in Seoul. In the NO-URBAN ensemble simulations, a large amount of condensates and strong updrafts are hardly found above  $z=6 \text{ km}$  (Figure 11c,d). This shows that convective cells in Seoul little develop into deep and strong storms in the NO-URBAN ensemble simulations. The amount of condensates and updraft intensity in the NO-UHI ensemble simulations are smaller than those in the NO-URBAN ensemble simulations (Figure 11e,f), indicating shallower and weaker developments of clouds likely contributed by urban dry island impacts in Seoul. In the NO-DRAG ensemble simulations, the amount of condensates and updraft intensity are comparable to those in the URBAN ensemble simulations (Figure 11g,h). This shows that deep and strong storms develop in Seoul in the NO-DRAG ensemble simulations, as in the URBAN ensemble simulations. These results indicate that the precipitation increase in Seoul by urban impacts is mainly attributed to the deeper and stronger developments of storms by the UHI impacts.

How the UHI impacts promote the developments of deep and strong storms in Seoul is examined. Figure 12a–d presents the PDFs of convective available potential energy (CAPE), density potential temperature and the magnitude of horizontal potential temperature gradient at the lowest model level, and vertical velocity at  $z=1 \text{ km}$  for the four sets of ensemble simulations. Here, the density potential temperature is calculated following Emanuel (1994). The CAPE in the URBAN, NO-UHI, and NO-DRAG ensemble simulations is smaller than that in the NO-URBAN ensemble simulations (Figure 12a). The larger CAPE in the NO-URBAN ensemble simulations is largely attributed to more abundant near-surface moisture without impervious urban surfaces, which was also reported by Rozoff et al. (2003). The PDFs of CAPE suggest that a possible increase in CAPE by the UHI impacts is not responsible for the developments of deep and strong storms in Seoul in the URBAN ensemble simulations. The UHI impacts on the storm development are closely associated with the enhanced updraft intensity initiated at the front of cold outflows. Compared with the NO-URBAN and NO-UHI ensemble simulations, in the URBAN and NO-DRAG ensemble simulations, the frequencies of high

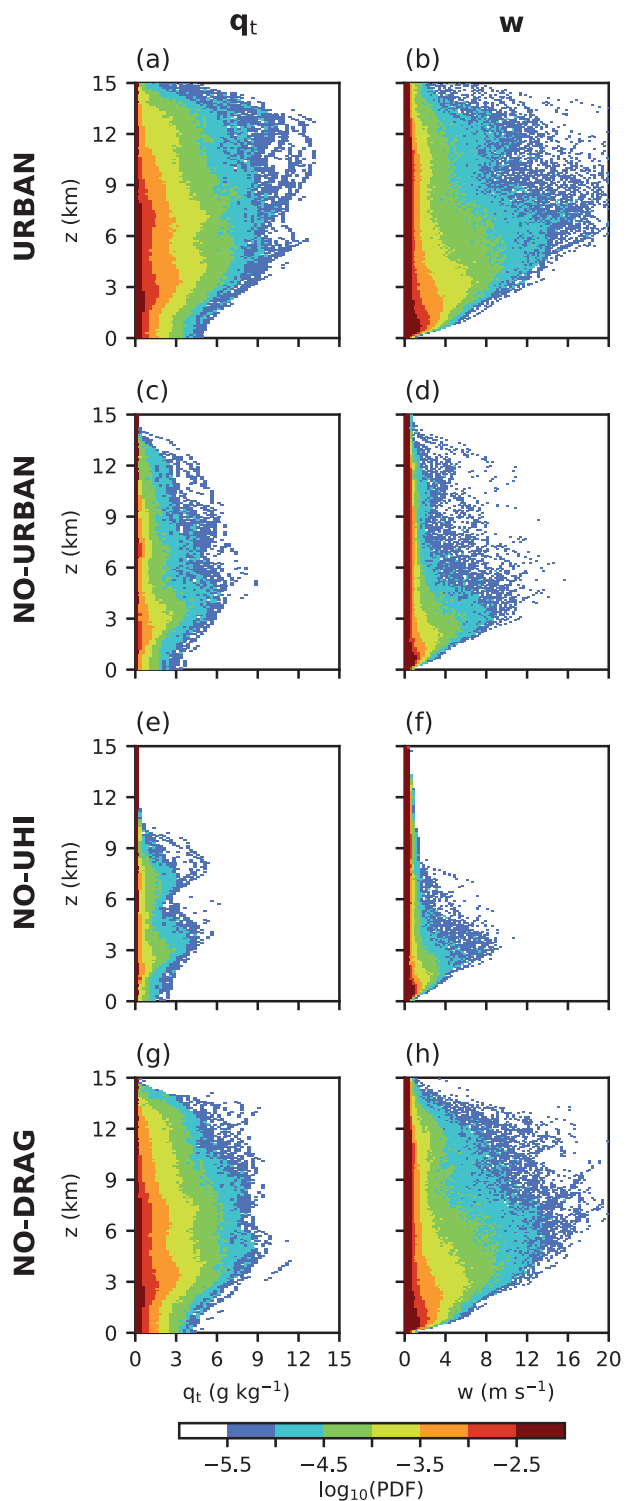


**FIGURE 11** Contoured frequency by altitude diagrams of (a,c,e,g) total water mixing ratio and (b,d,f,h) vertical velocity in the Seoul region (blue box in Figure 2b) during 1300–1700 LST for the (a,b) URBAN, (c,d) NO-URBAN, (e,f) NO-UHI, and (g,h) NO-DRAG ensemble simulations. [Colour figure can be viewed at [wileyonlinelibrary.com](http://wileyonlinelibrary.com)]

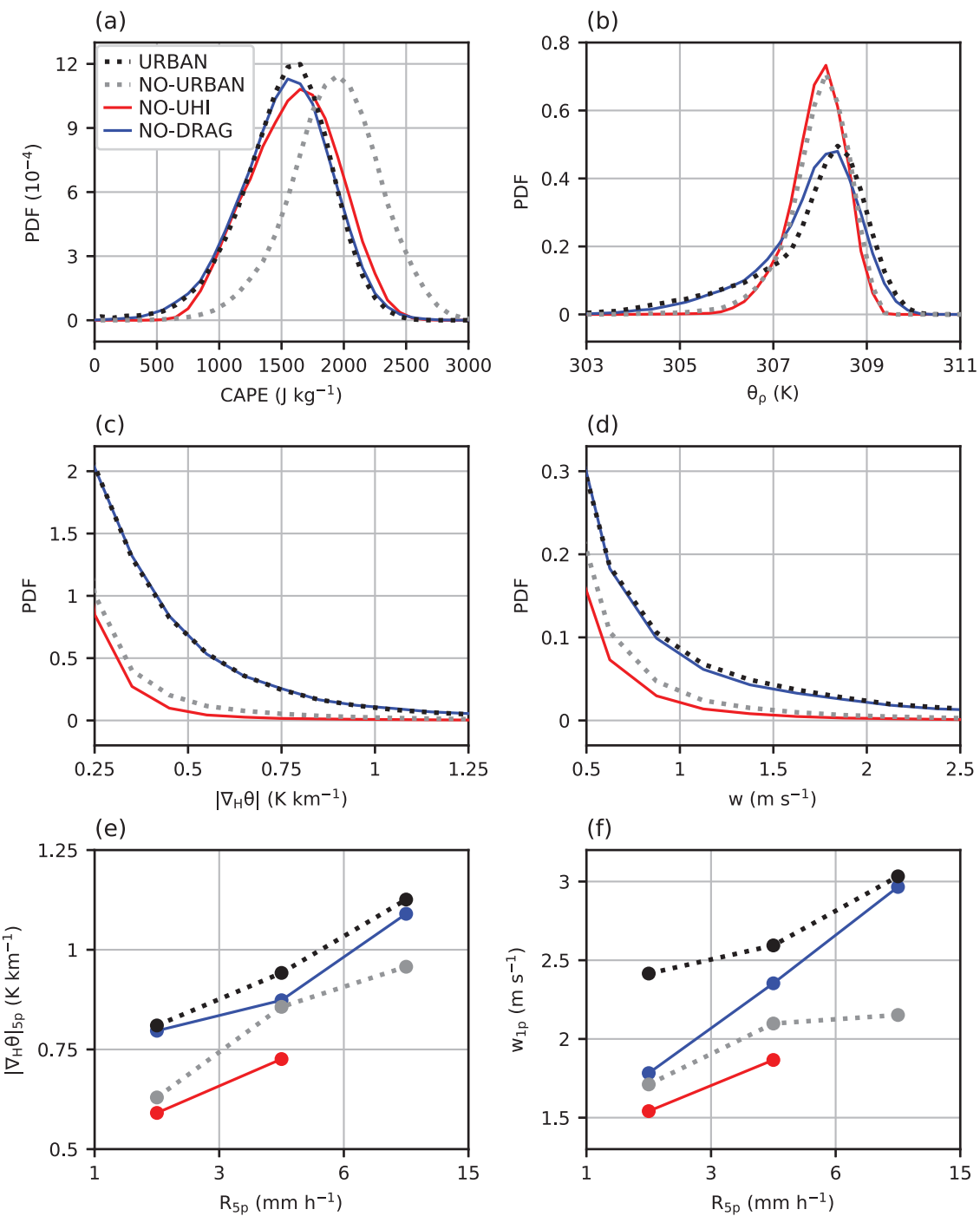


**FIGURE 12** PDFs of (a) CAPE, (b) density potential temperature and (c) the magnitude of horizontal potential temperature gradient at the lowest model level, and (d) vertical velocity at  $z = 1 \text{ km}$  in the Seoul region (blue box in Figure 2b) during 1300–1700 LST for the URBAN, NO-URBAN, NO-UHI, and NO-DRAG ensemble simulations. (e) Ensemble-mean upper 5 percentile magnitude of potential temperature gradient and (f) ensemble-mean upper 1 percentile vertical velocity for each category of ensemble-mean upper 5 percentile precipitation rate in the four sets of ensemble simulations. [Colour figure can be viewed at [wileyonlinelibrary.com](http://wileyonlinelibrary.com)]

( $> 309 \text{ K}$ ) and low ( $< 306 \text{ K}$ ) density potential temperatures are substantially increased (Figure 12b). These high or low potential temperatures are mainly associated with the UHI and precipitation-induced cold pool, respectively. The

larger horizontal contrasts of potential temperature lead to much stronger horizontal gradient of potential temperature (Figure 12c) which is mainly found near the front of cold outflows in the urban areas, as exemplified in

Figures 5–7. This stronger potential temperature gradient results in much stronger updrafts below the lifting condensation level in the URBAN and NO-DRAG ensemble simulations (Figure 12d).

The stronger potential temperature gradient and stronger updrafts near the front of cold outflows are not solely attributed to the stronger cold pool from stronger precipitation but also contributed by the warmer urban air due to the UHI in Seoul. Figure 12e,f shows the ensemble-mean upper 5 percentile magnitude of potential temperature gradient and ensemble-mean upper 1 percentile vertical velocity for each category of ensemble-mean upper 5 percentile precipitation rate in the four sets of ensemble simulations. Note that the mean magnitude of strong potential temperature gradient and the mean intensity of strong updrafts are larger in the URBAN and NO-DRAG ensemble simulations than in the NO-URBAN and NO-UHI ensemble simulations, even for the same category of the precipitation intensity in Seoul (Figure 12e,f). This indicates that the UHI increases the magnitude of potential temperature gradient and updraft intensity near the front of cold outflows from convective cells, which plays an important role in the development of initially weak convective cells into deep and strong storms in Seoul.

### 3.3 | Impacts of urban-topographic interaction on precipitation

The SMA has a complex geographical setting with the Yellow Sea west of the SMA, high mountains in the eastern SMA and east of the SMA, and modest mountains near Seoul. The impacts of these geographical elements can interact with urban impacts, affecting precipitation in the SMA. In this subsection, the impacts of interactions between urban impacts and topographic impacts on precipitation in this convective shower event are examined. For this, a set of ensemble simulations with the topography in the SMA being removed is conducted and called the NO-TOPO ensemble simulations. In these NO-TOPO ensemble simulations, terrain heights exceeding 100 m are set to 100 m in the main analysis region (Figure 1d). Outside of the main analysis region, a 20-km relaxation zone in which the original terrain heights are linearly recovered is considered. Another set of ensemble simulations in which the urban areas are replaced with croplands and the topography is removed in the same way in the main analysis region is conducted and called the NO-UBTP ensemble simulations.

To separately examine the urban impact alone, the topographic impact alone, and the impact of urban-topographic interaction on precipitation, the factor

**TABLE 2** Calculation methods for the contributions of the urban impact alone, the topographic impact alone, and the urban-topographic interaction impact on precipitation.

Contribution	Calculation method
Urban impact, without the interaction with topographic impact	NO-TOPO – NO-UBTP
Topographic impact, without the interaction with urban impact	NO-URBAN – NO-UBTP
Urban-topographic interaction impact	URBAN – (NO-URBAN + NO-TOPO) + NO-UBTP

separation analysis (Stein & Alpert, 1993) is conducted. The calculation methods for the contributions of the respective impacts to precipitation using the factor separation analysis are summarized in Table 2. The urban impact alone without the interaction with topographic impact is obtained by subtracting the result of the NO-UBTP ensemble simulations from that of NO-TOPO ensemble simulations. The topographic impact alone without the interaction with urban impact is obtained by subtracting the result of the NO-UBTP ensemble simulations from that of NO-URBAN ensemble simulations. The urban-topographic interaction impact is obtained by subtracting the urban impact alone from the urban impact with the interaction with topographic impact (URBAN – NO-URBAN, Figure 8c).

Figure 13 shows the spatial distributions of differences in accumulated precipitation amount caused by urban impact alone, topographic impact alone, and urban-topographic interaction impact. The urban impact alone increases precipitation by ~7 mm in a large portion of the Seoul region (Figure 13a). Meanwhile, the topographic impact alone increases precipitation in southwestern Seoul (Figure 13b), indicating that the storm in southwestern Seoul is generated by geographical influences even without urban impact. It is notable that the urban-topographic interaction impact significantly increases precipitation in northeastern Seoul by ~6 mm (Figure 13c) which is comparable to the increase due to the urban impact alone in this region (~7 mm) (Figure 13a). This indicates that the urban impact on precipitation for this convective shower event is amplified by interactions with topographic impact in the SMA. The topographic influences on winds in the western coast–Seoul region are presented in Figure 13d. In the morning, the easterly component is found below  $z \sim 1$  km, indicating the presence of mountain breeze. Meanwhile, in the early afternoon, the westerly component is found below  $z \sim 2$  km and the easterly component is found above it. These wind components are associated with circulation induced by moist

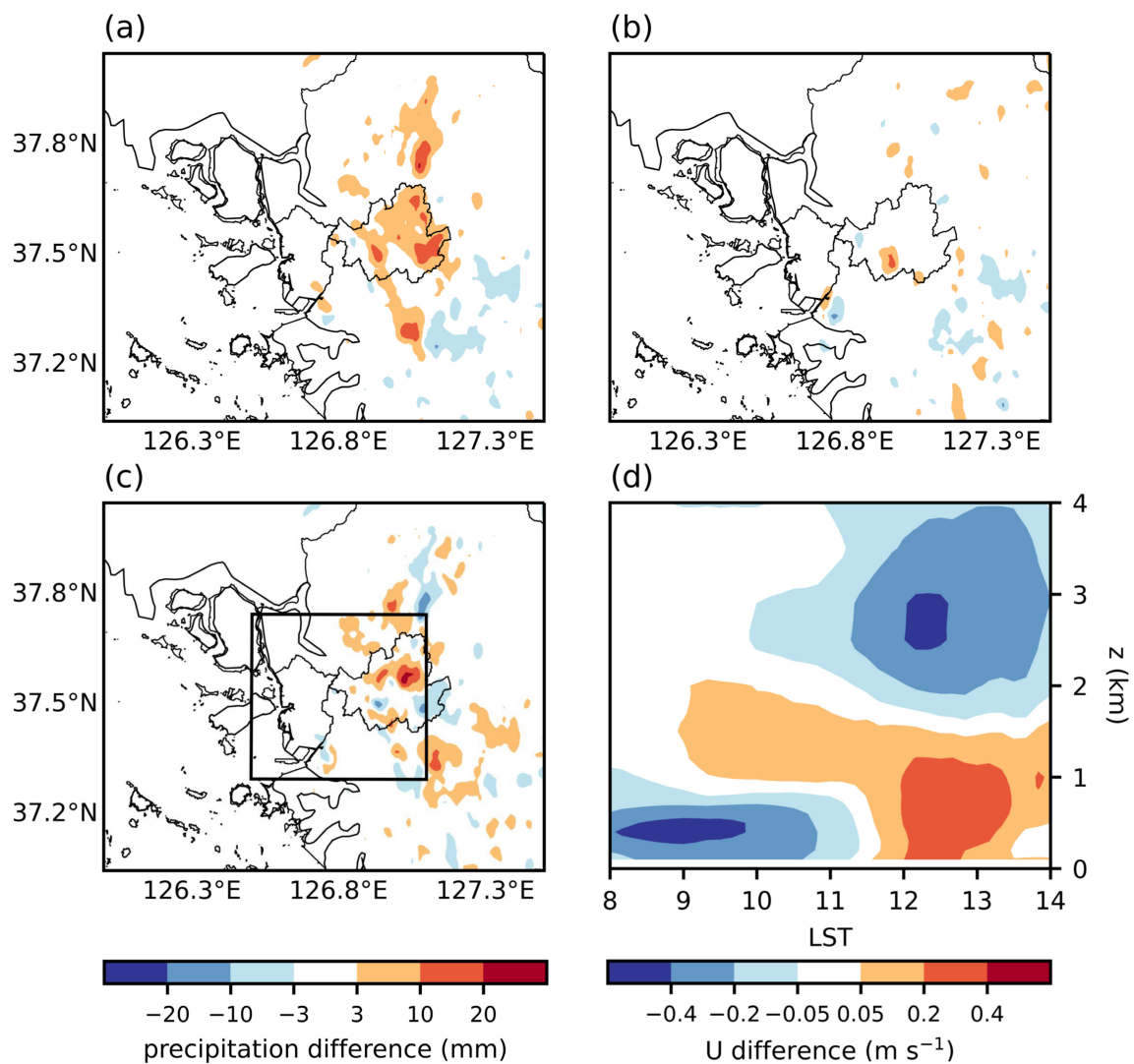


**FIGURE 13** Spatial distributions of differences in accumulated precipitation amount caused by (a) urban impact without interaction with topographic impact, (b) topographic impact without interaction with urban impact, and (c) urban–topographic interaction impact. The black box in (c) represents the western coast–Seoul region. (d) Time–height diagram of difference in  $x$ -directional wind averaged over the western coast–Seoul region between the URBAN and NO-TOPO ensemble simulations. [Colour figure can be viewed at [wileyonlinelibrary.com](http://wileyonlinelibrary.com)]

convection triggered over the high mountains in the eastern SMA.

To examine how convection developments are affected by topographic influences, the fields of local winds and precipitation in the SMA at 1230 LST for the URBAN and NO-TOPO ensemble simulations and their differences are presented in Figure 14a–c. The topography in the SMA is depicted by thin black contours. In the URBAN ensemble simulations (Figure 14a), precipitation occurs above the mountains in the eastern SMA, as well as southwest of Seoul near the western coast (orange arrow) and in western Seoul near the Han River (brown arrow). The development of moist convection above the mountains is associated with the short vertical distance from the mountain top to the lifting condensation level and mountain–plain

circulation (not shown). This moist convection is hardly found in the eastern SMA in the NO-TOPO simulations (Figure 14b), which leads to the wind differences in the SMA between the two sets of ensemble simulations (Figure 13d). It is notable that appreciable precipitation develops over the sea breeze front near the western border of Seoul (pink arrow) in the NO-TOPO ensemble simulations (Figure 14b), which is not found in the URBAN ensemble simulations (Figure 14a). In addition, the precipitation southwest of Seoul near the western coast (orange arrow) in the NO-TOPO ensemble simulations is stronger than that in the URBAN ensemble simulations, producing a stronger cold pool (Figure 14b,c).

The differences in moist convection development near the western border of Seoul and southwest of Seoul in

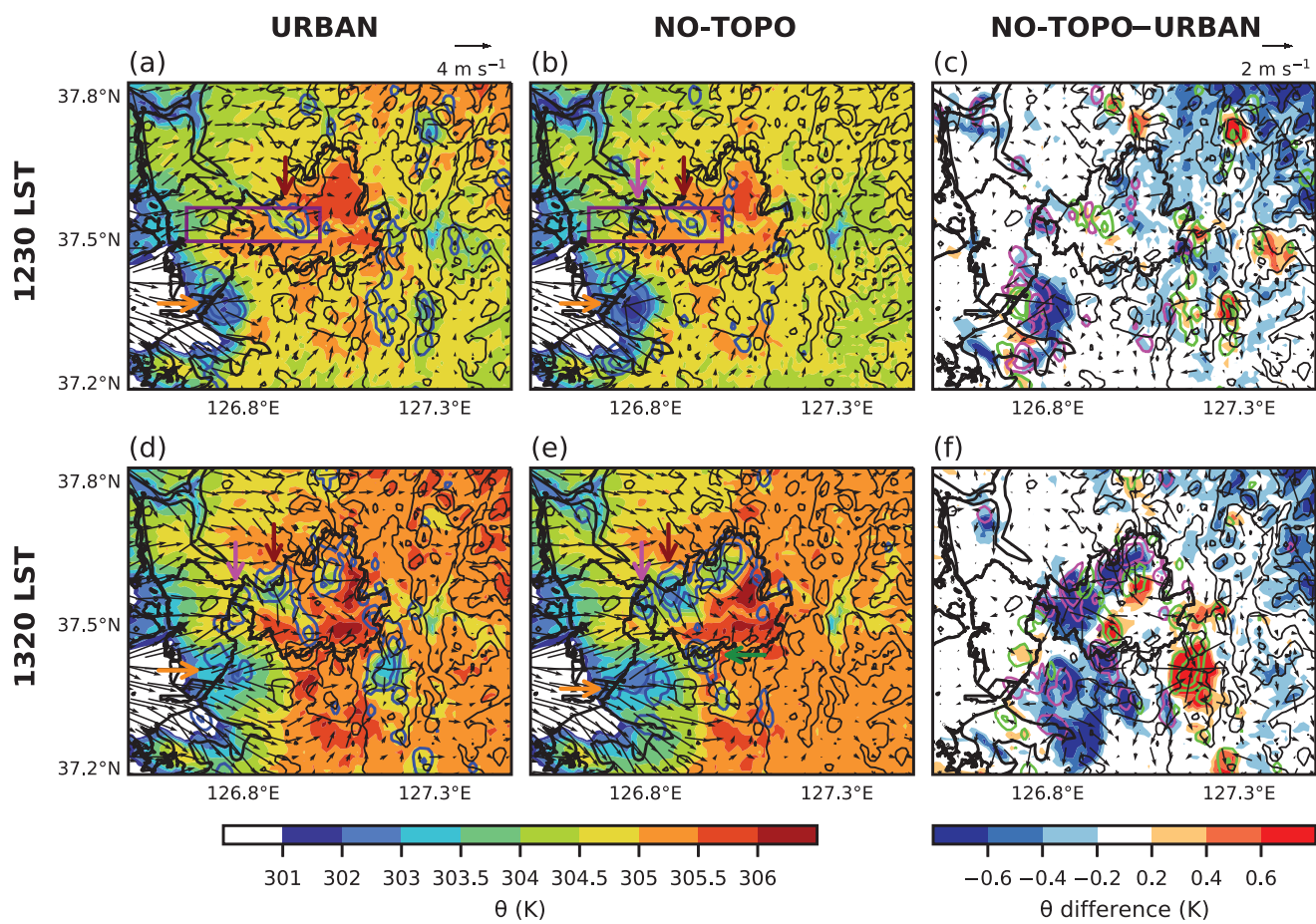


**FIGURE 14** Fields of potential temperature (shades) and wind vector (black arrows) at the lowest model level and precipitation rate (blue contours, at 0.5 and 4 mm·hr<sup>-1</sup>) at (a,b) 1230 and (d,e) 1320 LST for the (a,d) URBAN and (b,e) NO-TOPO ensemble simulations. The orange, brown, pink, and green arrows indicate the different convective cells explained in the text. The purple boxes represent the NW region which is used for the analysis in Figure 15. (c,f) Fields of differences in potential temperature (shades) and wind vector (black arrows) at the lowest model level and precipitation rate (pink contours, at 0.5 and 4 mm·hr<sup>-1</sup>; green contours, at -4 and -0.5 mm·hr<sup>-1</sup>) between the NO-TOPO and URBAN ensemble simulations at the same times. The topography of the URBAN ensemble simulations is depicted in all subfigures with thin black contours at 100, 300, 500, and 700 m. [Colour figure can be viewed at [wileyonlinelibrary.com](http://wileyonlinelibrary.com)]

the early afternoon lead to the urban-topographic interaction impact on precipitation in northeastern Seoul. Figure 14d-f is the same as Figure 14a-c but at 1320 LST. In the URBAN ensemble simulations (Figure 14d), the convective cells near the western border of Seoul (pink arrow) and in western Seoul near the Han River (brown arrow) produce moderate precipitation and weak cold pool, while in the NO-TOPO ensemble simulations (Figure 14e), the cells are relatively strongly developed and produce relatively stronger precipitation and cold pool. Note that the magnitude of the resultant potential temperature differences between the two sets of ensemble simulations in western Seoul is large, ranging from 0.5 to 1.2 K (Figure 14f). In the URBAN (NO-TOPO) ensemble simulations, the warmer (cooler) low-level air in western Seoul moves into central Seoul along with the sea breeze

and strengthens (weakens) storm development in northeastern Seoul in the late afternoon, which leads to the urban-topographic interaction impact on precipitation.

Meanwhile, the sea breeze southwest of Seoul enhanced by cold outflow (orange arrow) is stronger in the NO-TOPO ensemble simulations than in the URBAN ensemble simulations (Figure 14d,e). Hence, the sea breeze does not penetrate into southwestern Seoul yet in the URBAN ensemble simulations while it penetrates into southwestern Seoul and south of Seoul and produces significant precipitation there (green arrow) in the NO-TOPO ensemble simulations. The precipitation deficit (excess) southwest and south of Seoul in the early afternoon in the URBAN (NO-TOPO) ensemble simulations results in warmer (cooler) low-level air (Figure 14f) there, which later allows stronger (weaker) storm development in

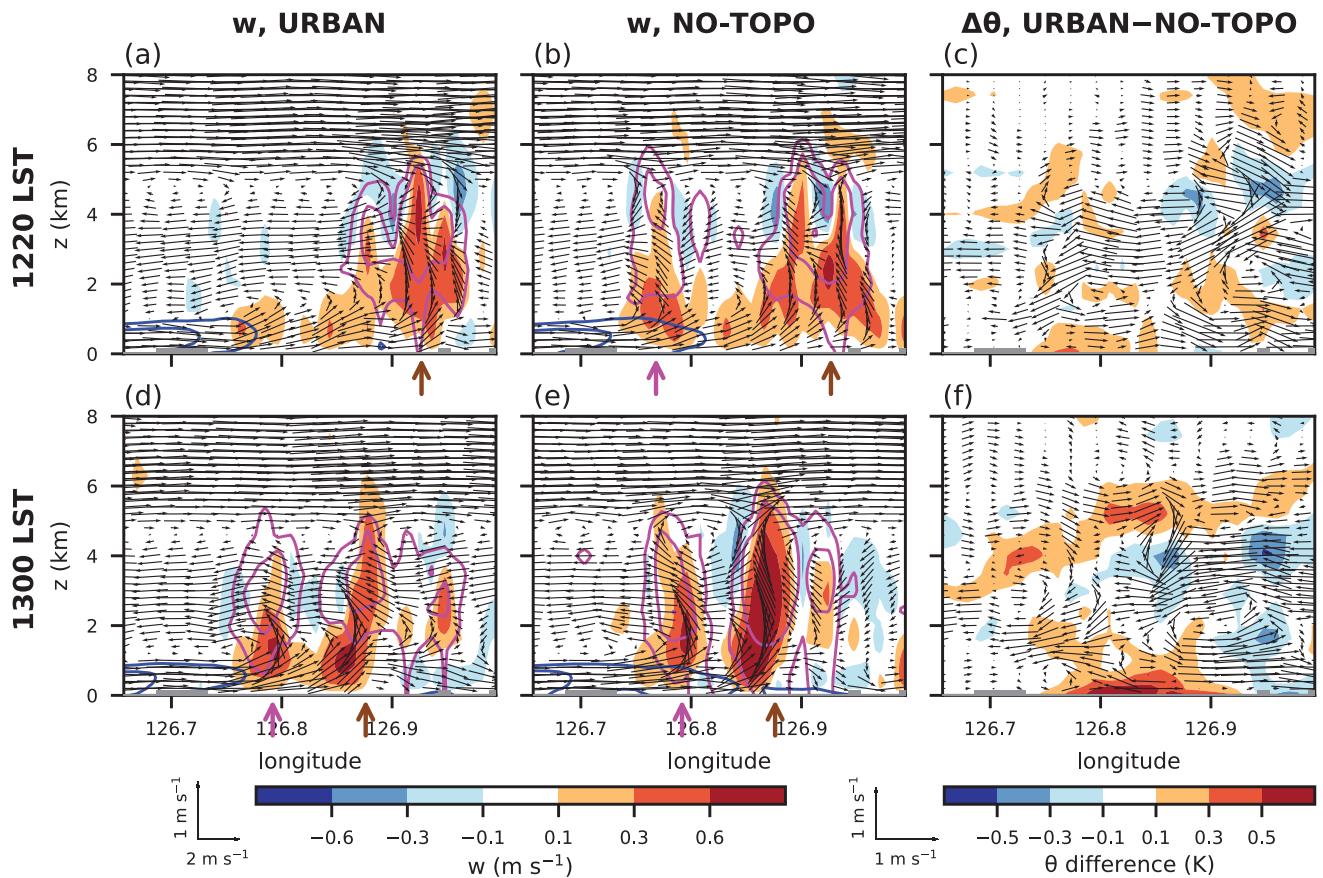


**FIGURE 15** Fields of vertical velocity (shades), total water mixing ratio (pink contours, at 0.05 and  $0.2 \text{ g} \cdot \text{kg}^{-1}$ ), wind vector (black arrows), and potential temperature (blue contours, at 304 and  $304.5 \text{ K}$ ) averaged over the  $y$ -direction in the NW region (purple box in Figure 14a,b) at (a,b) 1220 and (d,e) 1300 LST for the (a,d) URBAN and (b,e) NO-TOPO ensemble simulations. The pink and brown arrows indicate the different convective cells explained in the text. (c,f) Fields of differences in potential temperature (shades) and wind vector (black arrows) between the URBAN and NO-TOPO ensemble simulations at the same times. The gray-shaded areas in (a,c,d,f) and (b,e) represent the topography in the NW region for the URBAN and NO-TOPO ensemble simulations, respectively. The reference wind vectors for (a,b,d,e) and reference wind difference vectors for (c,f) are given in the bottom left and right, respectively. [Colour figure can be viewed at [wileyonlinelibrary.com](http://wileyonlinelibrary.com)]

southwestern Seoul and south of Seoul in the late afternoon. This affects storm development in northeastern Seoul as well, contributing to the urban-topographic interaction impact on precipitation. Overall, the results in Figure 14 indicate that topographic influences suppress the early-afternoon precipitation near the western coast and help to preserve the low-level warm air in the inland SMA, which leads to stronger storm development in Seoul in the late afternoon.

To understand how topographic influences result in the differences in moist convection development in western Seoul in the early afternoon, the evolution of local winds and convective cells in the NW region (purple box in Figure 14a,b) is compared between the URBAN and NO-TOPO ensemble simulations (Figure 15). At 1220 LST, the convective cells in western Seoul near the Han River (brown arrow) are found and the sea breeze (blue contours) blows from the west (Figure 15a,b). Note that

appreciable convective cells are not found over the sea breeze front near the western border of Seoul in the URBAN ensemble simulations while they are evident in the NO-TOPO ensemble simulations (pink arrow). The weaker development of convective cell over the sea breeze front in the URBAN ensemble simulations could be resulted from the stronger vertical shear due to the circulation associated with mountain-induced moist convection (Figures 13d and 15c). Adverse impacts of vertical wind shear having an opposite direction to the density current on convection development have been reported (e.g., Markowski & Richardson, 2010). The weaker development of convective cell over the sea breeze front in the URBAN ensemble simulations (pink arrow) leads to weaker precipitation in western Seoul (Figure 15d). Meanwhile, the stronger development of convective cell over the sea breeze front in the NO-TOPO ensemble simulations leads to stronger precipitation and stronger cold pool (Figure 15e)

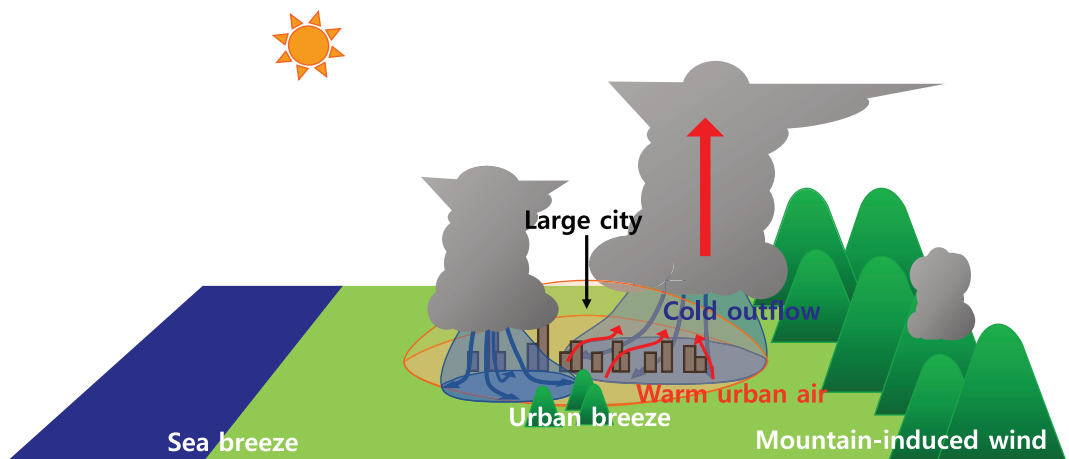


**FIGURE 16** Schematic diagram that depicts the important processes involved in the development of strong storms in Seoul for the scattered convective shower event. [Colour figure can be viewed at [wileyonlinelibrary.com](https://wileyonlinelibrary.com)]

that is clearly seen by a relatively warm anomaly in the URBAN ensemble simulations (Figure 15f). The lifting by this cold pool further intensifies the convective cell near the Han River (brown arrow), leading to stronger precipitation in western Seoul in the NO-TOPO ensemble simulations (Figure 15e).

The differences in moist convection development southwest and south of Seoul are also associated with the topographic impacts on local winds, as the differences near the western border of Seoul. The evolution of local winds and convective cells southwest and south of Seoul was examined in the URBAN and NO-TOPO ensemble simulations (not shown). The sea breeze southwest of Seoul in the late morning is weaker in the URBAN ensemble simulations than in the NO-TOPO ensemble simulations, due to the mountain breeze (Figure 13d). This contributes to weaker development of convective cell over the sea breeze front, leading to weaker development of later convective cells and precipitation southwest of Seoul in the early afternoon in the URBAN ensemble simulations. The examinations of local winds and convective cells near the western coast suggest that topographic influences on local winds near the western coast inhibit precipitation development by sea breeze in the early afternoon, eventually affecting storm development in the inland urban areas in the SMA.

The results of this study suggest that the circulation associated with mountain-induced moist convection modulates coastal convection development and influences the later developments of storms in inland urban areas. A similar but different way of interaction between urban impacts and mountain-induced circulation was suggested by Sun et al. (2021). Through ensemble simulations in the Great Bay Area, China with and without topography, they suggested that mountain–plain circulation increases near-surface wind speed and therefore enhances

sensible heat flux in the urban areas, which eventually intensifies the UHI intensity and UHI-induced precipitation enhancement. In our simulations, the temperature increase and the subsequent invigoration of storms are also found but the enhancement of urban sensible heat flux due to mountain-induced circulation is not found. Further investigations regarding impacts of urban–topographic interaction on precipitation are needed to better understand local processes associated with storm development in cities under complex geographical conditions.

## 4 | SUMMARY AND CONCLUSIONS

In this study, we examined urban impacts on storm development and precipitation and their interactions with topographic impacts for a convective shower event in the SMA through the different sets of ensemble simulations conducted using the WRF model. In the URBAN ensemble simulations, strong storms develop and produce precipitation in southwestern and northeastern Seoul. Meanwhile, in the NO-URBAN ensemble simulations, strong storms in northeastern Seoul do not develop and the precipitation amount in Seoul is significantly reduced to a fifth of that in the URBAN ensemble simulations. Comparisons with the NO-UHI and NO-DRAG ensemble simulations revealed that the UHI impacts play important roles in stronger storm development and resultant precipitation increases in Seoul. This stronger storm development by the UHI impacts is mainly attributed to the stronger updrafts at the front of cold outflows, rather than being attributed to the urban breeze circulation or an increase in CAPE resulting from the UHI. The urban drag impacts delay the precipitation evolution by ~1 hour in Seoul with a negligible effect on the precipitation amount. The factor separation

analysis based on the URBAN, NO-TOPO, NO-URBAN, and NO-UBTP ensemble simulations revealed that the urban-topographic interaction impact significantly contributes to the precipitation increase in northeastern Seoul, being indicative of the amplification of urban-induced increases in precipitation by topographic influences. This is attributed to the mountain-induced circulation which suppresses the development of coastal precipitation in the morning and therefore preserves the warm air that helps stronger development of the storms in Seoul in the late afternoon. The processes involved in the development of strong storms in Seoul for this convective shower event are summarized by a schematic diagram in Figure 16.

This study suggests that updraft enhancements by the UHI at the front of cold outflows can facilitate the development of strong storms, leading to precipitation enhancement in urban areas. This process is different from the other well-known processes arising from the UHI that can lead to precipitation, such as the UHI-induced circulation (e.g., Baik et al., 2001; Han & Baik, 2008) and the elevation of boundary layer top height (e.g., Li et al., 2017; Sun et al., 2021). In addition to these, other processes that are responsible for UHI-induced precipitation enhancement in and around cities under complex geographical conditions need to be revealed through further investigations of various precipitation cases.

This study examined the respective impacts of the UHI and urban drag on precipitation in the SMA. Previous studies have shown that urban aerosols can affect precipitation in and around a city (e.g., Fan et al., 2020; Han et al., 2012). Further investigation of the impacts of urban aerosols will be beneficial for the comprehensive understanding of urban impacts on precipitation in the SMA. This study examined the urban impacts on less-organized convective precipitation systems. Meanwhile, the urban impacts on highly organized or synoptic precipitation systems are also being actively investigated in recent years (Yue et al., 2021). In light of large contributions of strongly-forced precipitation systems to annual precipitation amounts in mid-latitude regions, understanding of the urban impacts on these systems and resultant precipitation could be particularly important for managements of flood risks and water resources in and around cities (Yang et al., 2019; Zhang et al., 2018). The urban impacts on highly organized or synoptic precipitation systems, particularly responsible processes therein, deserve in-depth investigation.

## ACKNOWLEDGEMENTS

The authors are grateful to two anonymous reviewers who helped improve this work by providing valuable comments. This work was supported by the National Research Foundation of Korea under grants 2021R1A2C1007044 and RS-2025-00562044.

## FUNDING INFORMATION

National Research Foundation of Korea, Grant Numbers: 2021R1A2C1007044 and RS-2025-00562044.

## CONFLICT OF INTEREST STATEMENT

The authors declare no conflict of interest.

## DATA AVAILABILITY STATEMENT

The data that support the findings of this study are available from the corresponding author upon reasonable request.

## ORCID

Jong-Jin Baik  <https://orcid.org/0000-0003-3709-0532>

## REFERENCES

- Argüeso, D., Luca, A.D. & Evans, J.P. (2016) Precipitation over urban areas in the western Maritime Continent using a convection-permitting model. *Climate Dynamics*, 47, 1143–1159.
- Baik, J.-J., Kim, Y.-H. & Chun, H.-Y. (2001) Dry and moist convection forced by an urban heat island. *Journal of Applied Meteorology*, 40, 1462–1475.
- Baik, J.-J., Kim, Y.-H., Kim, J.-J. & Han, J.-Y. (2007) Effects of boundary-layer stability on urban heat island-induced circulation. *Theoretical and Applied Climatology*, 89, 73–81.
- Bornstein, R. & LeRoy, M. (1990) Urban barrier effects on convective and frontal thunderstorms. In: *4th Conference on Mesoscale Processes, 25–29 June 1990, Boulder*. Boston: American Meteorological Society, pp. 120–121.
- Bretherton, C.S. & Park, S. (2009) A new moist turbulence parameterization in the Community Atmosphere Model. *Journal of Climate*, 22, 3422–3448.
- Changnon, S.A., Huff, F.A., Schickedanz, P.T. & Vogel, J.L. (1977) *Summary of METROMEX, volume 1: weather anomalies and impacts*. Urbana: Illinois State Water Survey.
- Chen, J., Theller, L., Gitau, M.W., Engel, B.A. & Harbor, J.M. (2017) Urbanization impacts on surface runoff of the contiguous United States. *Journal of Environmental Management*, 187, 470–481.
- Choi, Y. & Lee, Y.-H. (2021) Urban effect on sea-breeze-initiated rainfall: a case study for Seoul metropolitan area. *Atmosphere*, 12, 1483.
- Doan, Q.-V., Kobayashi, S., Kusaka, H., Chen, F., He, C. & Niyogi, D. (2023) Tracking urban footprint on extreme precipitation in an African megacity. *Journal of Applied Meteorology and Climatology*, 62, 209–226.
- Dou, J., Wang, Y., Bornstein, R. & Miao, S. (2015) Observed spatial characteristics of Beijing urban climate impacts on summer thunderstorms. *Journal of Applied Meteorology and Climatology*, 54, 94–105.
- Dudhia, J. (1989) Numerical study of convection observed during the Winter Monsoon Experiment using a mesoscale two-dimensional model. *Journal of the Atmospheric Sciences*, 46, 3077–3107.
- Emanuel, K.A. (1994) *Atmospheric convection*. New York: Oxford University Press.
- Fan, J., Rosenfeld, D., Zhang, Y., Giangrande, S.E., Li, Z., Machado, L.A.T. et al. (2018) Substantial convection and precipitation enhancements by ultrafine aerosol particles. *Science*, 359, 411–418.

- Fan, J., Zhang, Y., Li, Z., Hu, J. & Rosenfeld, D. (2020) Urbanization-induced land and aerosol impacts on sea-breeze circulation and convective precipitation. *Atmospheric Chemistry and Physics*, 20, 14163–14182.
- Forster, A., Augros, C. & Masson, V. (2024) Urban influence on convective precipitation in the Paris region: Hectometric ensemble simulations in a case study. *Quarterly Journal of the Royal Meteorological Society*, 150, 3028–3051.
- Freitag, B.M., Nair, U.S. & Niyogi, D. (2018) Urban modification of convection and rainfall in complex terrain. *Geophysical Research Letters*, 45, 2507–2515.
- Grimmond, C.S.B., Blackett, M., Best, M.J., Baik, J.-J., Belcher, S.E., Beringer, J. et al. (2011) Initial results from phase 2 of the international urban energy balance model comparison. *International Journal of Climatology*, 31, 244–272.
- Grimmond, C.S.B., Blackett, M., Best, M.J., Barlow, J., Baik, J.-J., Belcher, S.E. et al. (2010) The international urban energy balance models comparison project: first results from phase 1. *Journal of Applied Meteorology and Climatology*, 49, 1268–1292.
- Han, J.-Y. & Baik, J.-J. (2008) A theoretical and numerical study of urban heat island-induced circulation and convection. *Journal of the Atmospheric Sciences*, 65, 1859–1877.
- Han, J.-Y., Baik, J.-J. & Khain, A.P. (2012) A numerical study of urban aerosol impacts on clouds and precipitation. *Journal of the Atmospheric Sciences*, 69, 504–520.
- Han, J.-Y., Baik, J.-J. & Lee, H. (2014) Urban impacts on precipitation. *Asia-Pacific Journal of Atmospheric Sciences*, 50, 17–30.
- He, Y., Wang, J. & Feng, J. (2023) A typical weakly forced mountain-to-plain extreme precipitation event exacerbated by urbanization in Beijing. *Journal of Geophysical Research: Atmospheres*, 128, e2023JD039275.
- Hersbach, H., Bell, B., Berrisford, P., Hirahara, S., Horányi, A., Muñoz-Sabater, J. et al. (2020) The ERA5 global reanalysis. *Quarterly Journal of the Royal Meteorological Society*, 146, 1999–2049.
- Hong, S.-H., Jin, H.-G., Han, J.-Y. & Baik, J.-J. (2024) Initiation and evolution of urban-induced precipitation under different background wind speeds: roles of urban breeze circulation and cold pool. *Theoretical and Applied Climatology*, 155, 9457–9470.
- Hu, T., Wang, Y. & Wu, D. (2021) The interaction of an urban heat Island with a sea breeze front during moist convection over Tianjin, China. *Weather*, 77, 238–247.
- IPCC. (2023) *Climate change 2023: AR6 synthesis report*. Geneva: Intergovernmental Panel on Climate Change.
- Jensen, A.A., Harrington, J.Y., Morrison, H. & Milbrandt, J.A. (2017) Predicting ice shape evolution in a bulk microphysics model. *Journal of the Atmospheric Sciences*, 74, 2081–2104.
- Jiménez, P.A., Dudhia, J., González-Rouco, J.F., Navarro, J., Montávez, J.P. & García-Bustamante, E. (2012) A revised scheme for the WRF surface layer formulation. *Monthly Weather Review*, 140, 898–918.
- Jin, H.-G. & Baik, J.-J. (2025) Impacts of multi-physics ensemble on heavy precipitation prediction in South Korea: focusing on the performance of ensemble mean. *Meteorology and Atmospheric Physics*, 137, 35.
- Jongen, H.J., Lipson, M., Teuling, A.J., Grimmond, S., Baik, J.-J., Best, M. et al. (2024) The water balance representation in urban-PLUMBER land surface models. *Journal of Advances in Modeling Earth Systems*, 16, e2024MS004231.
- Kim, G., Cha, D.-H., Son, C.-K. & Kim, H. (2021) Impacts of anthropogenic heat and building height on urban precipitation over the Seoul metropolitan area in regional climate modeling. *Journal of Geophysical Research: Atmospheres*, 126, e2021JD035348.
- KOSIS. (2024) *Population Census*. Available from: <https://kosis.kr/index/index.do> [accessed 1 January 2025].
- Kusaka, H., Kimura, F., Nawata, K., Hanyu, T. & Miya, Y. (2009) The chink in the armor: Questioning the reliability of conventional sensitivity experiments in determining urban effects on precipitation patterns. In: *7th International Conference for Urban Climate, 29 June–03 July 2009, Yokohama*. Dublin: International Association for Urban Climate.
- Kusaka, H., Nawata, K., Suzuki-Parker, A., Takane, Y. & Furuhashi, N. (2014) Mechanism of precipitation increase with urbanization in Tokyo as revealed by ensemble climate simulations. *Journal of Applied Meteorology and Climatology*, 53, 824–839.
- Kusaka, H., Nishi, A., Mizunari, M. & Yokoyama, H. (2019) Urban impacts on the spatiotemporal pattern of short-duration convective precipitation in a coastal city adjacent to a mountain range. *Quarterly Journal of the Royal Meteorological Society*, 145, 2237–2254.
- Li, H., Cui, X. & Zhang, D.-L. (2017) Sensitivity of the initiation of an isolated thunderstorm over the Beijing metropolitan region to urbanization, terrain morphology and cold outflows. *Quarterly Journal of the Royal Meteorological Society*, 143, 3153–3164.
- Lim, K.-S.S. & Hong, S.-Y. (2010) Development of an effective double-moment cloud microphysics scheme with prognostic cloud condensation nuclei (CCN) for weather and climate models. *Monthly Weather Review*, 138, 1587–1612.
- Lin, C.-Y., Chen, W.-C., Chang, P.-L. & Sheng, Y.-F. (2011) Impact of the urban heat island effect on precipitation over a complex geographic environment in northern Taiwan. *Journal of Applied Meteorology and Climatology*, 50, 339–353.
- Lin, Y., Fan, J., Jeong, J.-H., Zhang, Y., Homeyer, C.R. & Wang, J. (2021) Urbanization-induced land and aerosol impacts on storm propagation and hail characteristics. *Journal of the Atmospheric Sciences*, 78, 925–947.
- Lipson, M.J., Grimmond, S., Best, M., Abramowitz, G., Coutts, A., Tapper, N. et al. (2024) Evaluation of 30 urban land surface models in the urban-PLUMBER project: phase 1 results. *Quarterly Journal of the Royal Meteorological Society*, 150, 126–169.
- Liu, J. & Niyogi, D. (2019) Meta-analysis of urbanization impact on rainfall modification. *Scientific Reports*, 9, 7301.
- Markowski, P. & Richardson, Y. (2010) *Mesoscale meteorology in Midlatitudes*. West Sussex: Wiley-Blackwell.
- Mlawer, E.J., Taubman, S.J., Brown, P.D., Iacono, M.J. & Clough, S.A. (1997) Radiative transfer for inhomogeneous atmospheres: RRTM, a validated correlated-k model for the longwave. *Journal of Geophysical Research*, 102, 16663–16682.
- MOIS. (2024) *2022 Disaster annual report*. Sejong City: Ministry of the Interior and Safety.
- Morrison, H. & Milbrandt, J.A. (2015) Parameterization of cloud microphysics based on the prediction of bulk ice particle properties. Part I: scheme description and idealized tests. *Journal of the Atmospheric Sciences*, 72, 287–311.
- Morrison, H., Thompson, G. & Tatarki, V. (2009) Impact of cloud microphysics on the development of trailing stratiform precipitation in a simulated squall line: comparison of one- and two-moment schemes. *Monthly Weather Review*, 137, 991–1007.
- Naylor, J. (2020) Idealized simulations of city-storm interactions in a two-dimensional framework. *Atmosphere*, 11, 707.

- Naylor, J. & Mulholland, J.P. (2023) The impact of vertical wind shear on the outcome of interactions between squall lines and cities. *Journal of Geophysical Research: Atmospheres*, 128, e2022JD037237.
- NCEI. (2024) U.S. Billion-Dollar Weather and Climate Disasters. Available from: <https://www.ncdc.noaa.gov/access/billions/state-summary/US> [accessed 1 January 2025].
- Oke, T.R., Mills, G., Christen, A. & Voogt, J.A. (2017) *Urban Climates*. Cambridge: Cambridge University Press.
- Reames, L.J. & Stensrud, D.J. (2018) Influence of a Great Plains urban environment on a simulated supercell. *Monthly Weather Review*, 146, 1437–1462.
- Rieck, M., Hohenegger, C. & Gentine, P. (2015) The effect of moist convection on thermally induced mesoscale circulations. *Quarterly Journal of the Royal Meteorological Society*, 141, 2418–2428.
- Rosenfeld, D. (2000) Suppression of rain and snow by urban and industrial air pollution. *Science*, 287, 1793–1796.
- Rozoff, C.M., Cotton, W.R. & Adegoke, J.O. (2003) Simulation of St. Louis, Missouri, land use impacts on thunderstorms. *Journal of Applied Meteorology*, 42, 716–738.
- Ryu, Y.-H. & Baik, J.-J. (2013) Daytime local circulations and their interactions in the Seoul metropolitan area. *Journal of Applied Meteorology and Climatology*, 52, 784–801.
- Ryu, Y.-H., Baik, J.-J. & Lee, S.-H. (2011) A new single-layer urban canopy model for use in mesoscale atmospheric models. *Journal of Applied Meteorology and Climatology*, 50, 1773–1794.
- Ryu, Y.-H., Baik, J.-J. & Lee, S.-H. (2012) Performance comparison of an urban canopy model under different meteorological conditions. *Atmosphere-Korea*, 22, 429–436.
- Schmid, P.E. & Niyogi, D. (2017) Modeling urban precipitation modification by spatially heterogeneous aerosols. *Journal of Applied Meteorology and Climatology*, 56, 2141–2153.
- Skamarock, W.C., Klemp, J.B., Dudhia, J., Gill, D.O., Liu, Z., Berner, J. et al. (2019) *A description of the advanced research WRF model version 4*. Boulder: National Center for Atmospheric Research.
- Stein, U. & Alpert, P. (1993) Factor separation in numerical simulations. *Journal of the Atmospheric Sciences*, 50, 2107–2115.
- Sun, X., Luo, Y., Gao, X., Wu, M., Li, M., Huang, L. et al. (2021) On the localized extreme rainfall over the Great Bay Area in South China with complex topography and strong UHI effects. *Monthly Weather Review*, 149, 2777–2801.
- Tewari, M., Chen, F., Wang, W., Dudhia, J., LeMone, M.A., Mitchell, K. et al. (2004) Implementation and verification of the unified Noah land surface model in the WRF model. In: *20th Conference on Weather Analysis and Forecasting/16th Conference on Numerical Weather Prediction*, 12–15 January 2004, Seattle. Boston: American Meteorological Society, pp. 11–15.
- Thompson, G., Field, P.R., Rasmussen, R.M. & Hall, W.D. (2008) Explicit forecasts of winter precipitation using an improved bulk microphysics scheme. Part II: Implementation of a new snow parameterization. *Monthly Weather Review*, 136, 5095–5115.
- UN. (2019) *World urbanization prospects: the 2018 revision*. New York: United Nations.
- WMO. (2021) *Atlas of mortality and economic losses from weather, climate and water extremes (1970–2019)*. Geneva: World Meteorological Organization.
- Wu, M., Luo, Y., Chen, F. & Wong, W.K. (2019) Observed link of extreme hourly precipitation changes to urbanization over coastal South China. *Journal of Applied Meteorology and Climatology*, 58, 1799–1819.
- Yang, L., Smith, J. & Niyogi, D. (2019) Urban impacts on extreme monsoon rainfall and flooding in complex terrain. *Geophysical Research Letters*, 46, 5918–5927.
- Yang, P., Ren, G. & Yan, P. (2017) Evidence for a strong association of short-duration intense rainfall with urbanization in the Beijing urban area. *Journal of Climate*, 30, 5851–5870.
- Yin, J., Zhang, D.-L., Luo, Y. & Ma, R. (2020) On the extreme rainfall event of 7 May 2017 over the coastal city of Guangzhou. Part I: impacts of urbanization and orography. *Monthly Weather Review*, 148, 955–979.
- Yue, C., Han, Z., Gu, W., Tang, Y. & Ao, X. (2021) Research progress for dynamic effects of cities on precipitation: a review. *Atmosphere*, 12, 1355.
- Zhang, W., Villarini, G., Vecchi, G.A. & Smith, J.A. (2018) Urbanization exacerbated the rainfall and flooding caused by hurricane Harvey in Houston. *Nature*, 563, 384–388.
- Zhang, W., Yang, J., Yang, L. & Niyogi, D. (2022) Impacts of city shape on rainfall in inland and coastal environments. *Earth's Future*, 10, e2022EF002654.

**How to cite this article:** Hong, S.-H. & Baik, J.-J. (2025) Urban impacts on deep convection development in the Seoul metropolitan area: A case modeling study of a scattered convective precipitation event. *Quarterly Journal of the Royal Meteorological Society*, 151:e5053. Available from: <https://doi.org/10.1002/qj.5053>